

Tanguy Mertens

A new mapped infinite partition of unity
method for convected acoustical radiation in
infinite domains.

January 20, 2009

Université Libre de Bruxelles

Remerciements

Si tu donnes un poisson à un homme, il ne mangera qu'un jour. S'il apprend à pêcher, il mangera toute sa vie.

Proverbe de Confucius, repris plus tard par Dominique Pire dans le cadre de l'action Iles de Paix.

Je remercie Philippe Bouillard de m'avoir donné ma canne à pêche et conduit à l'étang. Je remercie Laurent Hazard et Guy Paulus pour tous leurs conseils avisés. Et tous les autres, famille, amis, qui ont gardé confiance en moi et m'ont encouragé à la persévérance.

C'est grâce à vous tous que je peux vous présenter avec fierté mon premier poisson.

Ceci dit, je voudrais remercier de manière plus académique tous les acteurs du projet.

Je remercie Philippe Bouillard qui est à la source du projet et qui a contribué à mon épanouissement scientifique durant cette aventure au sein du service BATir. Je remercie également pour leur encadrement: Guy Warzée pour sa gentillesse et sa patience ainsi que Jean-Louis Migeot pour son soutien industriel et ses remarques pertinentes.

Ce passage au service BATir a été une expérience riche sur le plan scientifique mais aussi humain. Je remercie mes collègues de l'ULB pour les relations que nous avons construites ensemble, pour les activités dans le cadre du travail ou hors des murs de l'université. Je pense évidemment à Laurent Hazard et à Guy Paulus, pour leur amitié mais aussi leur disponibilité et leurs nombreux conseils. Merci aussi à tous les membres du service des milieux continus qui ont ajouté une dimension humaine. La nature des contrats de recherche et d'assistantat est tel qu'ils furent nombreux à être passés par les murs de l'université. Je ne pourrai tous les citer mais je tiens quand même à remercier personnellement Katy, Erik, Geneviève, Yannick, Louise, Dominique, Thierry, Sandrine, Bertha, David, Benoît, Peter et Kfir.

S'il est vrai qu'un travail de thèse tend à rendre le chercheur autonome, les collaborations et interactions restent importantes. Je remercie à cet égard toute l'équipe de l'Institute of Sound and Vibration Research de l'université de Southampton. Je remercie Jeremy Astley, chef du service de m'y avoir accueilli pendant un stage de six mois. Je le

remercie aussi pour l'environnement de travail de qualité qu'il m'a offert. Il est évident que la présence de Pablo Gamallo à l'I.S.V.R. a énormément contribué à l'aboutissement de ce travail de recherche. Je le remercie pour tout le temps qu'il m'a consacré, à Southampton et même par la suite lors de contacts e-mail ou lors de rencontres en conférences. Je le remercie pour l'intérêt qu'il porte à la présente étude, pour ses encouragements et pour tous ses enseignements. Mais ce séjour n'a pas été que professionnellement enrichissant, je repense à l'accueil qui m'a été réservé ainsi que de nombreux excellents souvenirs qui font de ce séjour une partie inoubliable de ma vie. Je tiens donc à remercier chaleureusement pour leur amitié précieuse Vincent et Theresa, Luigi, Claire, Naoki, Rie, Sue, Lisa, Eugene, Isa, Daniel et Stéphanie, Alessandro et Emmet.

Ces quelques lignes indiquent à quel point les relations humaines ont une influence sur ma vie. Cela ne sera pas une surprise alors si je remercie les personnes pour qui je *travaille dans les avions* ou ceux qui me félicitent de mon travail, *les semaines durant lesquelles, ils n'ont pas trop entendu les avions*. Je pense bien entendu à ma famille, principalement ma maman, pour avoir fait de moi l'homme que je suis aujourd'hui et mes amis, plus particulièrement mes colocataires: Iyad, Mathieu, Quentin, Guerrick, Caroline et Florence. Merci à vous de partager mes valeurs et de colorier mon existence.

Enfin, je terminerai par remercier les deux petits rayons de soleil qui ont ensoleillé la fin de ce long parcours.

List of Symbols

Greek symbols

β	: $\sqrt{1 - M_0^2}$	
γ	: Poisson ratio of specific heat capacities : c_p/c_v	
Γ	: interface separating the inner and the outer domains	
ε	: Error	
μ	: phase function	[m]
ρ	: mass density	[kgm ⁻³]
ρ_0	: steady mean density	[kgm ⁻³]
ρ_a	: acoustic density	[kgm ⁻³]
σ	: stress tensor	[Nm ⁻²]
ϕ	: velocity potential	[m ² s ⁻¹]
ϕ_0	: mean velocity potential	[m ² s ⁻¹]
ϕ_a	: acoustic velocity potential	[m ² s ⁻¹]
$\tilde{\phi}_a$: amplitude of the harmonic acoustic velocity potential	[m ² s ⁻¹]
$\tilde{\phi}^h$: numerical approximation of $\tilde{\phi}_a$	[m ² s ⁻¹]
$\tilde{\phi}_h^I$: numerical approximation in the outer region Ω_o	[m ² s ⁻¹]
Φ_α	: shape function for the α^{th} degree of freedom	
Φ_α^I	: infinite shape function for the α^{th} degree of freedom	
ω	: angular frequency	[s ⁻¹]
Ω	: domain	
Ω_i	: inner region	
Ω_o	: outer region	

Arabic symbols

\tilde{a}_n	: normal acceleration of a vibrating wall	$[ms^{-2}]$
A_n	: normal acoustic admittance	$[m^2skg^{-1}]$
A_{mn}^\pm	: incident and reflected modal amplitude	$[m^2s^{-1}]$
c	: speed of sound	$[ms^{-1}]$
c_0	: steady mean part of the speed of sound	$[ms^{-1}]$
c_∞	: speed of sound at large distance from the source	$[ms^{-1}]$
c_p	: specific heat capacity at constant pressure	$[JK^{-1}]$
c_v	: specific heat capacity at constant volume	$[JK^{-1}]$
$dofs$: number of unknowns of the approximation	
E	: energy flow out of a surface	$[J]$
E_{mn}^\pm	: incident and reflected modal pattern	
f	: excitation frequency	$[s^{-1}]$
G	: geometric factor	
h	: mesh size	$[m]$
H	: Hilbert space	
i	: imaginary unit = $\sqrt{-1}$	
\mathbf{I}	: Sound intensity	$[Wm^{-2}]$
J'	: stagnation entropy	$[Jkg^{-1}]$
k	: wavenumber	$[m^{-1}]$
$k_{r,mn}^\pm$: incident and reflected radial wavenumber	$[m^{-1}]$
k_B	: Boltzmann constant	$[JK^{-1}]$
$K_{z,mn}^\pm$: incident and reflected axial wavenumber	$[m^{-1}]$
L_j^d	: Legendre polynomial of order d for node j	
L_s	: curve enclosing the boundary S_s	
L_v	: curve enclosing the boundary S_v	
m	: angular mode number	
\mathbf{m}'	: mass flux	$[kgm^{-2}s^{-1}]$
m_0	: radial order of the infinite element	
m_w	: mass of a molecule	$[kg]$
M_0	: mach number	
M_i	: Mapping function for node/point i	
\mathbf{n}	: outer normal to the domain	
n	: radial mode number	
n_d^I	: number of infinite degree of freedom	
$n(j)$: size of the local approximation space at node j	
nni	: number of infinite nodes	
$nodes$: number of nodes	
N_i	: Partition of Unity function of node i	
N_m	: number of angular modes	
N_n	: number of radial modes	
N_M	: number of reflected modes (unknown)	

p	: fluid pressure	$[Pa]$
p_0	: steady mean fluid pressure	$[Pa]$
p_a	: acoustic pressure	$[Pa]$
\tilde{p}_a	: amplitude of the harmonic acoustic pressure	$[Pa]$
\tilde{p}_{an}	: analytic amplitude of the harmonic acoustic pressure	$[Pa]$
\mathbf{q}	: heat flux	$[Wm^{-2}]$
Q_w	: heat production	$[J]$
r_o	: distance to the source point	$[m]$
R	: specific gas constant	$[JK^{-1}mol^{-1}]$
R_j	: radial function for infinite node j	
R_j^d	: radial function of order d for node j	
s	: entropy	$[Jkg^{-1}K^{-1}]$
S	: boundary	
S_i	: mapping functions for the interface Γ	
S_M	: Modal boundary	
S_s	: soft wall	
S_v	: vibrating wall	
t	: time	$[s]$
T	: Temperature	$[K]$
T_j	: circumferential function for infinite node j	
\tilde{u}_n	: normal displacement of a vibrating wall	$[m]$
\mathbf{v}	: fluid velocity	$[ms^{-1}]$
\mathbf{v}_0	: steady mean fluid velocity	$[ms^{-1}]$
\mathbf{v}_∞	: fluid velocity at large distance from the source	$[ms^{-1}]$
\mathbf{v}_a	: acoustic velocity	$[ms^{-1}]$
$\tilde{\mathbf{v}}_a$: amplitude of the harmonic acoustic velocity	$[ms^{-1}]$
\mathcal{V}	: the Sobolev space $W^{1,2} = H^1 = \{f : f, \nabla f \in L^2\}$	
V_{jl}	: l^{th} local approximation function of node j	
\tilde{w}_n	: normal velocity of a vibrating wall	$[ms^{-1}]$
W_j	: weight function of node j	
W_j^I	: infinite weight function of the infinite node j	
$W_{M, nm}$: modal weight function of the angular and radial mode (m, n)	

Operators

∇	: gradient operator
$\nabla \cdot$: divergence operator
$\nabla \times$: curl operator
Δ	: Laplacian operator
$\frac{D}{Dt}$: Total time derivative
$:$: the double dot product of two tensors
$\langle \rangle$: time average
\Re	: Real part

Contents

1	Introduction	13
2	Formulation	17
2.1	Convected wave equation	18
2.2	Variational formulation	22
2.3	Boundary conditions	23
2.3.1	Vibrating wall boundary condition	23
2.3.2	Admittance boundary condition	25
2.4	Literature review of numerical methods	27
2.5	Partition of Unity Method	29
2.6	Modal and transmitted boundary conditions	35
2.6.1	Propagation in a straight duct	35
2.6.2	Modal coupling	42
2.7	Unbounded applications: state of the art	44
2.8	Mapped Infinite Partition of Unity Elements	46
2.8.1	Radial functions	48
2.8.2	Outwardly propagating wavelike factor	49
2.8.3	Circumferential functions	50
2.8.4	Infinite shape and weighting functions	51
2.9	Axisymmetric formulation	53
2.9.1	The Partition of Unity Method	55

2.9.2	Application of the boundary conditions	57
2.9.3	Mapped Infinite Partition of Unity Elements	62
2.10	Summary	66
3	Axisymmetric formulation: Verification tests	67
3.1	Duct propagation	67
3.1.1	Propagating mode in a hard walled duct	68
3.1.2	Evanescent mode in a hard walled duct	70
3.1.3	Propagating mode in a lined duct	72
3.1.4	Convected propagation in a hard walled duct	74
3.1.5	Convected propagation in a lined duct	75
3.2	Propagation in a non-uniform duct	77
3.3	Multipole radiation	79
3.4	Rigid piston radiation	82
3.5	Radiation of an infinitesimal cylinder within a uniform mean flow	83
4	Three-dimensional formulation: Verification tests	89
4.1	Duct propagation	89
4.2	Multipole radiation	94
5	Axisymmetric formulation: performance analysis	97
5.1	Duct propagation	98
5.1.1	Convergence and performance analyses	98
5.1.2	Local enrichment	105
5.1.3	Conditioning	108
5.2	Multipole radiation	113
5.2.1	Infinite element parameters	113
5.2.2	Dipole radiation: performance analysis	117
5.2.3	Multipole $N = 7$ radiation: performance analysis	120
5.3	Rigid piston radiation	122
5.4	Conclusion	124

6	Three-dimensional formulation: performance analysis	129
6.1	Duct propagation	129
6.1.1	Circular cross-section	129
6.1.2	Rectangular cross-section	133
6.1.3	Annular cross-section	134
6.1.4	Conclusion	136
6.2	Multipole radiation	136
7	Aliasing error	141
7.1	One-dimensional case	143
7.2	Two-dimensional case	146
8	Industrial application: Turbofan radiation	149
8.1	Radiation without flow	152
8.2	Convected radiation	155
8.3	Convected radiation and influence of liners	158
9	Conclusions	159
10	Appendices	163
10.1	Mapping functions	163
10.1.1	Three-dimensional mapping	163
10.1.2	Two-dimensional mapping	164
10.2	Modes in a two-dimensional lined duct with uniform mean flow along the duct axis	165
10.3	Outwardly propagating wavelike factor	166
10.4	Effect of uniform mean flow on plane wave propagation	167
10.5	Local enrichment: Application to the multipole	169
	References	171

Formulation

This chapter addresses the formulation of acoustic wave propagation within a flow in a domain $\Omega \in \mathbb{R}^n$ ($n = 1 : 3$). The relations are valid for the propagation in an unbounded region and for indoor applications (bounded domains).

The sound field is considered as small perturbations of the flow, small compared to the corresponding mean flow quantities. These acoustic perturbations represent the propagation of a wave and are chosen to have a time-harmonic variation.

We first establish the convected wave equation, by considering a compressible inviscid perfect isentropic irrotational gas flow. The unknown of this equation is the acoustic velocity potential which is linked to the particle acoustic velocity, hence to the acoustic pressure. The variational formulation is then derived from this equation by a weighted residual method as procedure.

The basic equations and assumptions are described in section 2.1. The most interesting result of this section is the convected wave equation which is a scalar partial differential equation expressing the propagation of acoustic waves traveling in an irrotational mean flow. Since it is not possible to solve this equation analytically for common applications, a computational method is derived from the variational formulation of the convected wave equation (section 2.2) for which typical wall boundary conditions are presented in section 2.3.

A literature review of available numerical methods is given at section 2.4. We detail the Partition of Unity Finite Element Method (section 2.5), leading to the matrix system to solve. This section is followed by the prescription of modal boundary conditions (section 2.6). Their conditions are not presented with the classical wall boundary conditions since the author considered it easier, for comprehension, to explain them after introducing the approximation scheme and the matrix formulation.

An additional numerical treatment has to be taken into account to deal with unbounded applications. A literature review about these techniques is given at section 2.7. The Mapped Infinite Partition of Unity Method, the selected treatment, is presented in section 2.8.

The complete three-dimensional computational method has been expressed in an axisymmetric formulation (section 2.9). This allows to save computational time when the geometry of the application can be obtained by revolution.

2.1 Convected wave equation

The convected wave equation describes the propagation of an acoustic wave within a flow. This equation is based on fundamental relations such as mass and momentum conservation equations. The motion of fluids are based on the continuum approximation. This means that flow quantities are smooth functions in (\mathbf{x}, t) . The convected wave equation is obtained under a number of assumptions for the fluid and the flow field.

- The fluid is an ideal gas.
- It is considered in a local thermodynamic equilibrium.
- The fluid is non viscous and is non heat-conducting.
- Flow quantities can be separated in steady mean flow contributions and their harmonic acoustic perturbations, where mean flow is uniform at large distance from the source.
- Gravity forces are neglected.

These assumptions correspond to a compressible perfect isentropic irrotational gas flow. The previous notions are detailed in this section. The following equations that will be used in the formulation have been inspired by references [67, 44, 36, 37, 38, 17].

The mass conservation is given by:

$$\frac{\partial \rho}{\partial t} + \nabla \cdot (\rho \mathbf{v}) = 0 \quad (2.1)$$

where ρ is the mass density of the flow, t is the time and \mathbf{v} is the fluid velocity vector.

The momentum equation is:

$$\frac{D\mathbf{v}}{Dt} = -\frac{\nabla p}{\rho} \quad (2.2)$$

since we neglected the gravity forces and considered a non viscous fluid. The total derivative $(\frac{D}{Dt})$ is defined by:

$$\frac{D}{Dt} = \frac{\partial}{\partial t} + \mathbf{v} \cdot \nabla \quad (2.3)$$

The energy equation is:

$$\rho T \frac{Ds}{Dt} = -\nabla \cdot \mathbf{q} + \boldsymbol{\sigma} : \nabla \mathbf{v} + Q_w \quad (2.4)$$

where T is the temperature, \mathbf{q} is the heat flux, Q_w is the heat production per volume unit and $\boldsymbol{\sigma}$ the stress tensor. Since we assumed no heat sources are present and the heat transfer and viscous dissipation are negligible, the flow is isentropic $\frac{Ds}{Dt} = 0$. We also assume the flow being uniform at large distance which lead to a uniform entropy $\nabla s = 0$. This is called homentropic flow.

The three main flow quantities are related by the ideal gas law:

$$p = \rho RT \quad (2.5)$$

where p is the pressure, R is the specific gas constant, the ratio $R = \frac{k_B}{m_w}$ of the constant of Boltzmann k_B and the mass of a molecule m_w . Since we assume a local thermodynamic equilibrium for the flow, this implies for a homogeneous fluid that two intrinsic state variables fully determine the state of the fluid (e.g. : s, ρ). Then:

$$dp = \left(\frac{\partial p}{\partial \rho} \right)_s d\rho + \left(\frac{\partial p}{\partial s} \right)_\rho ds \quad (2.6)$$

The flow is defined as isentropic ($ds = 0$), the speed of sound is defined by:

$$c = \sqrt{\left(\frac{\partial p}{\partial \rho} \right)_s} \quad (2.7)$$

For homentropic flows, the thermodynamic process is adiabatic:

$$p = K \rho^\gamma \quad (2.8)$$

where $\gamma = \frac{c_p}{c_v}$ is the Poisson ratio of the specific heat capacities at constant pressure and constant volume, respectively.

Equation 2.7 becomes:

$$c = \sqrt{\gamma \frac{p}{\rho}} \quad (2.9)$$

or, by using equation 2.8:

$$c^2 = \gamma K \rho^{\gamma-1} \quad (2.10)$$

We restrict the flow to be irrotational. This means that the flow velocity vector \mathbf{v} can be obtained from the scalar velocity potential ϕ :

$$\mathbf{v} = \nabla \phi \quad (2.11)$$

Considering equations 2.3 and 2.11, momentum equation 2.2 becomes:

$$\nabla \left(\frac{\partial \phi}{\partial t} + \frac{\nabla \phi \cdot \nabla \phi}{2} + \int \frac{dp}{\rho} \right) = 0 \quad (2.12)$$

By using equation 2.8, the integral part becomes:

$$\int \frac{dp}{\rho} = \frac{c^2}{\gamma - 1} \quad (2.13)$$

We can write the so-called Bernoulli equation 2.14 from equations 2.12 and 2.13:

$$\frac{\partial \phi}{\partial t} + \frac{v^2}{2} + \frac{c^2}{\gamma - 1} = \frac{v_\infty^2}{2} + \frac{c_\infty^2}{\gamma - 1} \quad (2.14)$$

with $v^2 = \mathbf{v} \cdot \mathbf{v}$, c_∞ and \mathbf{v}_∞ being respectively the sound speed and the fluid velocity vector at large distance from the acoustic sources where we assume the flow to be uniform.

The flow quantities are decomposed in their steady mean flow $(\)_0$ and harmonic acoustic $(\)_a$ parts:

$$\rho = \rho_0 + \rho_a \quad (2.15)$$

$$p = p_0 + p_a \quad (2.16)$$

$$\mathbf{v} = \mathbf{v}_0 + \mathbf{v}_a \quad (2.17)$$

$$\phi = \phi_0 + \phi_a \quad (2.18)$$

Note that acoustic perturbations are small compared to mean flow quantities. Equation 2.14 can be rewritten as:

$$c^2 = c_\infty^2 - (\gamma - 1) \left(\frac{\partial \phi_a}{\partial t} + \frac{\partial \phi_0}{\partial t} + \frac{v_0^2 - v_\infty^2}{2} + \mathbf{v}_0 \cdot \nabla \phi_a + \frac{\nabla \phi_a \cdot \nabla \phi_a}{2} \right) \quad (2.19)$$

With the assumption that the uniform flow is stationary, neglecting second order terms and exploiting equation 2.10, equation 2.19 becomes:

$$K\gamma(\rho_0 + \rho_a)^{\gamma-1} = c_0^2 \left(1 - \frac{\gamma - 1}{c_0^2} \left(\frac{\partial \phi_a}{\partial t} + \mathbf{v}_0 \cdot \nabla \phi_a \right) \right) \quad (2.20)$$

where we define c_0 as:

$$c_0^2 = c_\infty^2 - (\gamma - 1) \left(\frac{v_0^2 - v_\infty^2}{2} \right) \quad (2.21)$$

Then:

$$\rho_a = -\rho_0 + \left(\frac{c_0^2}{K\gamma} \right)^{\frac{1}{\gamma-1}} \left(1 - \frac{\gamma - 1}{c_0^2} \left(\frac{\partial \phi_a}{\partial t} + \mathbf{v}_0 \cdot \nabla \phi_a \right) \right)^{\frac{1}{\gamma-1}} \quad (2.22)$$

Equation 2.22 can be expressed as follows:

$$\rho_a = -\rho_0 + \rho_0 \left(1 - \frac{\gamma - 1}{c_0^2} \left(\frac{\partial \phi_a}{\partial t} + \mathbf{v}_0 \cdot \nabla \phi_a \right) \right)^{\frac{1}{\gamma-1}} \quad (2.23)$$

Then, developing the last term of equation 2.23 with a Taylor series, we finally obtain:

$$\rho_a = -\frac{\rho_0}{c_0^2} \left(\frac{\partial \phi_a}{\partial t} + \mathbf{v}_0 \cdot \nabla \phi_a \right) \quad (2.24)$$

or,

$$\rho_a = -\frac{\rho_0}{c_0^2} \frac{D\phi_a}{Dt} \quad (2.25)$$

The relation between the acoustic pressure and the acoustic potential is obtained from the previous relation 2.25 by considering the linearized thermodynamic relation 2.7:

$$p_a = -\rho_0 \frac{D\phi_a}{Dt} \quad (2.26)$$

Taking into account the multiple scale decomposition, the mass conservation equation 2.1 becomes:

$$\frac{\partial \rho_0}{\partial t} + \frac{\partial \rho_a}{\partial t} + \nabla \cdot (\rho_0 \mathbf{v}_0) + \nabla \cdot (\rho_0 \mathbf{v}_a) + \nabla \cdot (\rho_a \mathbf{v}_0) + \nabla \cdot (\rho_a \mathbf{v}_a) = 0 \quad (2.27)$$

As we assume that the mean flow is stationary, the first term of equation 2.27 is equal to zero. The last term of the same equation is neglected. This equation is then decomposed in a zero order (equation 2.28) and a first order (equation 2.29) equations. The zero order equation can be used to solve the irrotational mean flow. This equation is non linear because the mean flow density ρ_0 depends on the mean flow velocity \mathbf{v}_0 . It has to be solved iteratively.

$$\begin{cases} \nabla \cdot (\rho_0 \mathbf{v}_0) = 0 \\ \frac{v_0^2}{2} + \frac{\rho_0^{(\gamma-1)} K \gamma}{\gamma-1} = \frac{v_\infty^2}{2} + \frac{c_\infty^2}{\gamma-1} \end{cases} \quad (2.28)$$

$$\frac{\partial \rho_a}{\partial t} + \nabla \cdot (\mathbf{v}_0 \rho_a) + \nabla \cdot (\rho_0 \nabla \phi_a) = 0 \quad (2.29)$$

Combining equations 2.29 and 2.25, we obtain the convected wave equation. In the following, we assume the mean flow quantities to be known, such that the only unknown is the acoustic velocity potential.

$$-\frac{\partial}{\partial t} \left(\frac{\rho_0}{c_0^2} \frac{D\phi_a}{Dt} \right) - \nabla \cdot \left(\frac{\rho_0}{c_0^2} \frac{D\phi_a}{Dt} \mathbf{v}_0 \right) + \nabla \cdot (\rho_0 \nabla \phi_a) = 0 \quad (2.30)$$

The small acoustic perturbations are considered harmonic:

$$\phi_a(\mathbf{x}, t) = \Re \left(\tilde{\phi}_a(\mathbf{x}) e^{i\omega t} \right) \quad (2.31)$$

where $\omega = 2\pi f$ is the angular frequency and f is the excitation frequency.

The convected wave equation 2.30 becomes:

$$\begin{aligned} & \nabla \cdot \left(\rho_0 \nabla \tilde{\phi}_a - \frac{\rho_0}{c_0^2} \left(\mathbf{v}_0 \cdot \nabla \tilde{\phi}_a \right) \mathbf{v}_0 \right) \\ & - i\omega \left(\frac{\rho_0}{c_0^2} \mathbf{v}_0 \cdot \nabla \tilde{\phi}_a + \nabla \cdot \left(\frac{\rho_0}{c_0^2} \tilde{\phi}_a \mathbf{v}_0 \right) \right) \\ & + \frac{\omega^2 \rho_0}{c_0^2} \tilde{\phi}_a = 0 \end{aligned} \quad (2.32)$$

2.2 Variational formulation

The variational formulation is obtained by using a standard weighted residual procedure for equation (2.32). The domain Ω is surrounded by a boundary S ; W is a weight function and \mathcal{V} the Sobolev space $W^{1,2} = H^1 = \{f : f, \nabla f \in L^2\}$.

Integrating the product of the convected wave equation times a weight function leads to:

$$\begin{aligned} & \int_{\Omega} W \nabla \cdot \left(\rho_0 \nabla \tilde{\phi}_a - \frac{\rho_0}{c_0^2} \left(\mathbf{v}_0 \cdot \nabla \tilde{\phi}_a \right) \mathbf{v}_0 - i\omega \frac{\rho_0}{c_0^2} \tilde{\phi}_a \mathbf{v}_0 \right) d\Omega \\ & - \int_{\Omega} i\omega W \left(\frac{\rho_0}{c_0^2} \mathbf{v}_0 \cdot \nabla \tilde{\phi}_a \right) d\Omega + \int_{\Omega} \frac{\omega^2 \rho_0}{c_0^2} W \tilde{\phi}_a d\Omega = 0 \quad \forall W \in \mathcal{V} \end{aligned} \quad (2.33)$$

The first term is rewritten using the identity, $\mathbf{F} \cdot \nabla a = \nabla(\mathbf{F}a) - a\nabla \cdot \mathbf{F}$:

$$\begin{aligned} & \int_{\Omega} \nabla \cdot \left(\rho_0 W \nabla \tilde{\phi}_a - \frac{\rho_0}{c_0^2} W \left(\mathbf{v}_0 \cdot \nabla \tilde{\phi}_a \right) \mathbf{v}_0 - i\omega \frac{\rho_0}{c_0^2} W \tilde{\phi}_a \mathbf{v}_0 \right) d\Omega \\ & - \int_{\Omega} \left(\rho_0 \nabla \tilde{\phi}_a - \frac{\rho_0}{c_0^2} \left(\mathbf{v}_0 \cdot \nabla \tilde{\phi}_a \right) \mathbf{v}_0 - i\omega \left(\frac{\rho_0}{c_0^2} \tilde{\phi}_a \mathbf{v}_0 \right) \right) \cdot \nabla W d\Omega \\ & - \int_{\Omega} i\omega W \left(\frac{\rho_0}{c_0^2} \mathbf{v}_0 \cdot \nabla \tilde{\phi}_a \right) d\Omega + \int_{\Omega} \frac{\omega^2 \rho_0}{c_0^2} W \tilde{\phi}_a d\Omega = 0 \quad \forall W \in \mathcal{V} \end{aligned} \quad (2.34)$$

Following the divergence theorem applied to the first integral of the previous relation 2.34:

$$\begin{aligned}
& - \int_{\Omega} \left(\rho_0 \nabla \tilde{\phi}_a - \frac{\rho_0}{c_0^2} (\mathbf{v}_0 \cdot \nabla \tilde{\phi}_a) \mathbf{v}_0 \right) \cdot \nabla W d\Omega \\
& - i\omega \int_{\Omega} \frac{\rho_0}{c_0^2} \left(W \mathbf{v}_0 \cdot \nabla \tilde{\phi}_a - \tilde{\phi}_a \mathbf{v}_0 \cdot \nabla W \right) d\Omega + \omega^2 \int_{\Omega} \frac{\rho_0}{c_0^2} W \tilde{\phi}_a d\Omega \\
& = \int_S \frac{\rho_0}{c_0^2} W (\mathbf{v}_0 \cdot \nabla \tilde{\phi}_a) \mathbf{n} \cdot \mathbf{v}_0 dS - \int_S \rho_0 W \mathbf{n} \cdot \nabla \tilde{\phi}_a dS \\
& + i\omega \int_S \left(\frac{\rho_0}{c_0^2} W \tilde{\phi}_a \mathbf{v}_0 \cdot \mathbf{n} \right) dS \quad \forall W \in \mathcal{V}
\end{aligned} \tag{2.35}$$

where \mathbf{n} is the normal of the boundary, chosen to be pointing outside the domain Ω .

In the following, we consider three-dimensional applications. The domain Ω is a volume of fluid and the boundary S is a surface. Some three-dimensional applications have special geometrical and flow properties. This is taken into account (section 2.9) and leads to an axisymmetric formulation.

2.3 Boundary conditions

The integral over the boundary S allows for prescribing boundary conditions. It corresponds to the acoustic mass flow rate $\int_S (\rho_0 \mathbf{v}_a + \rho_a \mathbf{v}_0) \cdot \mathbf{n} dS$ but it is not a usual quantity to prescribe. In common applications, the boundary is composed of a number of walls which may vibrate or be covered by an absorbing material. This leads in flow respectively to vibrating wall, and Myers (or admittance) boundary conditions. The Myers boundary condition [39] allows to represent absorbing walls (such as curtains, liners, etc.) in presence of mean flow. Instead of walls, the boundary can also represent the outlet of a duct radiating in the domain Ω . It is then convenient to create the modal boundary condition which enables to prescribe incident and reflected duct modes.

2.3.1 Vibrating wall boundary condition

We consider vibrating walls as a part of the boundary $S_v \in S$ which moves harmonically relative to a given frame with a normal displacement to the reference $u_n = \tilde{u}_n e^{i\omega t}$. The vibration is prescribed by giving the normal displacement of the wall \tilde{u}_n but it can also be done by giving its normal velocity $w_n = \tilde{w}_n e^{i\omega t}$ or normal acceleration $a_n = \tilde{a}_n e^{i\omega t}$, as they are related by:

$$\tilde{u}_n = -\frac{i\tilde{w}_n}{\omega} = -\frac{\tilde{a}_n}{\omega^2} \quad (2.36)$$

We assume that there are no voids at the wall interface and that the steady mean flow velocity \mathbf{v}_0 is tangent to the undeformed stationary boundary (the boundary is an impermeable wall thus the normal mean flow velocity is null $\mathbf{v}_0 \cdot \mathbf{n} = 0$).

Considering the last assumption and the relation $\nabla \tilde{\phi}_a = \tilde{\mathbf{v}}_a$, leads to a simplification of the boundary integral of the weak formulation 2.35.

$$\begin{aligned} & \int_{S_v} \frac{\rho_0}{c_0^2} W \left(\mathbf{v}_0 \cdot \nabla \tilde{\phi}_a \right) \mathbf{n} \cdot \mathbf{v}_0 dS - \int_S \rho_0 W \mathbf{n} \cdot \nabla \tilde{\phi}_a dS \\ & + i\omega \int_{S_v} \left(\frac{\rho_0}{c_0^2} W \tilde{\phi}_a \mathbf{v}_0 \cdot \mathbf{n} \right) dS \\ & = - \int_{S_v} \rho_0 W \tilde{\mathbf{v}}_a \cdot \mathbf{n} dS \end{aligned} \quad (2.37)$$

The Myers expression [39] given at expression 2.38 expresses the proper impenetrable boundary condition on the acoustic field in the presence of a base flow. It links the normal part of the acoustic flow velocity $\tilde{\mathbf{v}}_a \cdot \mathbf{n}$ to the normal displacement \tilde{u}_n of the vibrating wall S_v . This equation assumes the fluid to be inviscid and implies the continuity of particle displacement and pressure through an infinitely thin boundary layer.

$$\tilde{\mathbf{v}}_a \cdot \mathbf{n} = i\omega \tilde{u}_n + \mathbf{v}_0 \cdot \nabla \tilde{u}_n - \tilde{u}_n \mathbf{n} \cdot (\mathbf{n} \cdot \nabla) \mathbf{v}_0 \quad (2.38)$$

The boundary integral takes a form which is not convenient as it requires both the gradient of the wall displacement and the gradient of the mean flow velocity. A more suitable form has been proposed by Eversman [41]. It is based on the Myers expression modified by the use of some vector identities and previous relations.

$$\begin{aligned} \rho_0 W \mathbf{v}_0 \cdot \nabla \tilde{u}_n &= \rho_0 \mathbf{v}_0 \cdot \nabla (W \tilde{u}_n) - \rho_0 \tilde{u}_n \mathbf{v}_0 \cdot \nabla W \\ &= \nabla \cdot (W \rho_0 \mathbf{v}_0 \tilde{u}_n) - W \tilde{u}_n \nabla \cdot (\rho_0 \mathbf{v}_0) - \rho_0 \tilde{u}_n \mathbf{v}_0 \cdot \nabla W \\ &= \nabla \cdot (W \rho_0 \mathbf{v}_0 \tilde{u}_n) - \rho_0 \tilde{u}_n \mathbf{v}_0 \cdot \nabla W \end{aligned} \quad (2.39)$$

As

$$\nabla \cdot (\rho_0 \mathbf{v}_0) = 0$$

and, since $\mathbf{v}_0 \cdot \mathbf{n} = 0$; the following equation holds

$$\begin{aligned} \rho_0 W \tilde{u}_n \mathbf{n} \cdot (\mathbf{n} \cdot \nabla) \mathbf{v}_0 &= \mathbf{n} \cdot (\mathbf{n} \cdot \nabla) (\rho_0 W \tilde{u}_n \mathbf{v}_0) - \mathbf{v}_0 \cdot \mathbf{n} (\mathbf{n} \cdot \nabla) (\rho_0 W \tilde{u}_n) \\ &= \mathbf{n} \cdot (\mathbf{n} \cdot \nabla) (\rho_0 W \tilde{u}_n \mathbf{v}_0) \end{aligned} \quad (2.40)$$

Considering these relations and the fact that $\mathbf{n} \cdot \mathbf{n} = 1$ and that the vector triple product $(\mathbf{a} \times (\mathbf{b} \times \mathbf{c})) = (\mathbf{a} \cdot \mathbf{c}) \mathbf{b} - (\mathbf{a} \cdot \mathbf{b}) \mathbf{c}$, the boundary integral 2.37 becomes:

$$\begin{aligned}
-\int_{S_v} \rho_0 W \tilde{\mathbf{v}}_a \cdot \mathbf{n} dS &= -\int_{S_v} (i\omega \rho_0 W \tilde{u}_n - \rho_0 \tilde{u}_n \mathbf{v}_0 \cdot \nabla W) dS \\
&\quad - \int_{S_v} (\nabla \cdot (W \rho_0 \mathbf{v}_0 \tilde{u}_n) - \mathbf{n} \cdot (\mathbf{n} \cdot \nabla) (\rho_0 W \tilde{u}_n \mathbf{v}_0)) dS \\
&= -\int_{S_v} (i\omega \rho_0 W \tilde{u}_n - \rho_0 \tilde{u}_n \mathbf{v}_0 \cdot \nabla W) dS \\
&\quad - \int_{S_v} \mathbf{n} \cdot \nabla \times (\mathbf{n} \times (W \rho_0 \mathbf{v}_0 \tilde{u}_n)) dS \tag{2.41}
\end{aligned}$$

As it is explained by Eversman in [41], the use of Stokes' theorem on the last boundary integral term leads to a line integral 2.42 over L_v which should enclose the boundary S_v . In general, the vibrating wall is surrounded by a hard wall, like it is the case for a piston (fig. 2.1). Then, there is a curve (L_v) over which the integral 2.42 vanishes as the displacement of a hard wall is null.

$$\begin{aligned}
-\int_{S_v} \mathbf{n} \cdot \nabla \times (\mathbf{n} \times (W \rho_0 \mathbf{v}_0 \tilde{u}_n)) dS &= -\int_{L_v} (\mathbf{n} \times (W \rho_0 \mathbf{v}_0 \tilde{u}_n)) \cdot dL \\
&= 0 \text{ if } \tilde{u}_n = 0 \text{ on } L_v \tag{2.42}
\end{aligned}$$

By considering equation 2.41, we can remark that boundary integral for a hard wall is null as the displacement is null over the whole wall.

2.3.2 Admittance boundary condition

Contrary to hard walls, soft walls (such as curtains, liners, ...) react to the acoustic pressure. The velocity of the soft wall (S_s) is linked to the acoustic pressure through the normal admittance coefficient (A_n) where $A_n = a + ib$ is a complex number (see equation 2.44). This coefficient depends on the material covering the wall.

We assume that the soft wall is impermeable to the flow $\mathbf{v}_0 \cdot \mathbf{n} = 0$ and that the Myers boundary condition 2.38 links the normal acoustic flow velocity $\mathbf{v}_a \cdot \mathbf{n}$ to the wall displacement u_n . The main assumption to obtain Myers expression [39] consists in the continuity of the particle displacement through an infinitely thin boundary layer. Then the previous development for the boundary integral in the case of a vibrating wall can be

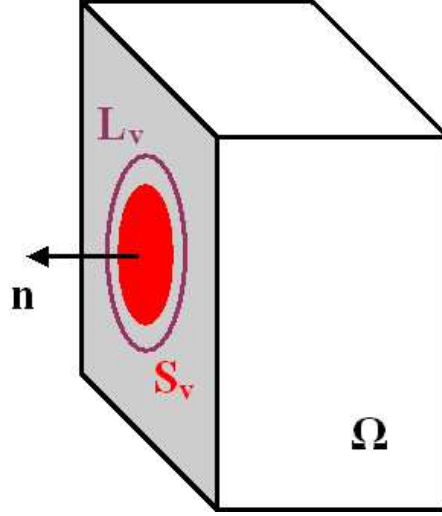


Fig. 2.1. Representation of a vibrating piston (in red: S_v) included in a hard wall (in grey).

followed to obtain equation 2.41, as it has been done by Eversman [41]. Then by considering that the displacement of the soft wall is related to the material property A_n and the acoustic potential $\tilde{\phi}_a$ given in equation 2.44, the boundary integral over the soft wall becomes:

$$\begin{aligned}
-\int_{S_s} \rho_0 W \tilde{\mathbf{v}}_a \cdot \mathbf{n} dS &= \int_{S_s} A_n \rho_0^2 \left(W \mathbf{v}_0 \cdot \nabla \tilde{\phi}_a - \tilde{\phi}_a \mathbf{v}_0 \cdot \nabla W \right) dS \\
&+ i\omega \int_{S_s} A_n \rho_0^2 \tilde{\phi}_a W dS \\
&- \frac{1}{i\omega} \int_{S_s} A_n \rho_0^2 \left(\mathbf{v}_0 \cdot \nabla \tilde{\phi}_a \right) \left(\mathbf{v}_0 \cdot \nabla W \right) dS \\
&+ \int_{L_s} \mathbf{n} \times \left(\frac{A_n \rho_0^2 W \mathbf{v}_0}{i\omega} \left(i\omega \tilde{\phi}_a + \mathbf{v}_0 \cdot \tilde{\phi}_a \right) \right) \cdot dL \quad (2.43)
\end{aligned}$$

as

$$\begin{aligned}
\tilde{w}_n &= A_n \tilde{p}_a \\
\tilde{u}_n &= -\frac{A_n}{i\omega} \rho_0 \left(i\omega \tilde{\phi}_a + \mathbf{v}_0 \cdot \nabla \tilde{\phi}_a \right) \quad (2.44)
\end{aligned}$$

The previous remark concerning the line integration also stands here. If there exists a surrounding curve (L_s) lying on a hard wall, this line integral vanishes.

2.4 Literature review of numerical methods

A common approach for simulating turbofan noise radiation in the frequency domain is the use of the Finite Element Method, typically with linear or quadratic shape functions. Note that these simulations could also be performed in the time domain with a mathematical model based on the Linearized Euler Equations (LEE) by the use of the Dispersion Relation Preserving (DRP) scheme [82] or the Discontinuous Galerkin Method (DGM) [87]. The frequency domain Finite Element Method is effective for axisymmetric models at moderate frequencies but for three-dimensional models the simulation is limited to a range of frequencies which does not include all the contributions needed for realistic applications. The Finite Element Method is a deterministic approach in which the calculation domain is meshed such that the waves can be represented accurately by polynomial shape functions. This means that meshes are frequency dependent. A general rule of the thumb which is widely used advocates the use of 6 to 10 linear elements to approximate a wavelength in the solution. This rule has the virtue of simplicity, but has been shown to be invalid for short wavelength problems for which Ihlenburg and others [1, 2, 3, 4] have shown that the error (in relative H_1 semi-norm) of the acoustic finite element solution for the Helmholtz equation is composed of two terms, interpolation (a) and pollution error (b):

$$\varepsilon_{|H_1} = \underbrace{C_1(p) \left(\frac{kh}{2p}\right)^o}_{(a)} + \underbrace{C_2(p) k \left(\frac{kh}{2p}\right)^{o+1}}_{(b)} \quad (kh \leq \alpha < \pi) \quad (2.45)$$

where $\varepsilon_{|H_1}$ is the error in H_1 semi-norm, (C_1, C_2) are constants which does not depend on the wavenumber k nor the size of the mesh h , p the polynomial order of the shape functions (this notation may be confusing with the notation p corresponding to the fluid pressure) and $o = \min(l, p)$ if we assume that the exact solution is of regularity $l + 1$. The proof has been carried out for *constant resolution*, i.e. under the assumption $kh \leq \alpha$. Equation (2.45) shows that keeping the term kh constant while increasing the frequency is not sufficient to ensure a constant error. The effect of this relation is that the mesh should contain more than the classic 6 to 10 elements per wavelength when applied to shortwave problems in acoustics, such as turbofan radiation, where many wavelengths of the solution are contained within the computational domain. This requires of course very large amount of computer resources. For this reason, O.C. Zienkiewicz [5] classified in the year 2000 short wave computations as unsolved problems for the finite element method.

Several methods have been proposed to reduce the numerical error of deterministic methods, see Thompson [6] for a recent review. The basic idea is, whatever the formulation, to improve the interpolation scheme. An active field of research is based on the inclusion of a priori solution in the approximation, i.e. local set of plane waves.

The first way is to enrich the existing Finite Element approximation. In the case of the Partition of Unity Finite Element Method [7, 8, 9], the Finite Element functions are multiplied by local enrichment functions which can be polynomial, trigonometric, etc. The

Generalized Finite Element Method [10, 11, 12, 13] is based on the same principles except that the approximation is the combination of polynomial finite element and Partition of Unity function. The Discontinuous Enrichment Method [14] separates the unknown field in two scales, the first one (called coarse scale) constructed by piecewise polynomial Finite Element functions and the fine scale, chosen to be particular solutions of the problem. The fine scale is allowed to be discontinuous across element boundaries and the continuity is then forced by Lagrange multipliers.

With the same objective, the Trefftz formulation presented in 1926 has been re-examined by Desmet et al. under the name Wave Based Method [15]. The approximation is assumed to be purely composed of local solutions of the problem within each element (plane waves). No volume integration has to be performed, only integrals over the boundary to prescribe boundary conditions and inter-elements boundaries to guarantee the continuity of the solution. Gamallo and Astley [16] compared two Trefftz methods for wave problems based on the Ultra Weak Variational Formulation [19, 20] and the Least Square Method [21]. The Ultra Weak Variational formulation uses integration by parts to derive a variational formulation that weakly enforces appropriate continuity conditions between elements via impedance boundary condition. While the Least Square Method enforces the continuity across element boundaries by minimizing the least square difference of the solution and its derivative. Gabard [54] shows that the Ultra Weak Variational Formulation is in fact a subset of the Discontinuous Galerkin Method [55] with plane waves (note that the Discontinuous Galerkin Method is in fact a variant of the Discontinuous Enrichment Method for which the polynomial field is dropped).

Huttunen, Gamallo and Astley [18] compared the Partition of Unity Finite Element method locally enriched with a set of plane waves to the Ultra Weak Variational Formulation. In the Ultra Weak Variational Formulation, the approximation is purely constructed with a set of plane waves while the Partition of Unity Finite Element approximation incorporates polynomial component. Both methods give high level of accuracy even with coarse meshes ($\lambda/h = 0.3$ lead to 0.01% of error). These method reach tolerable accuracy for a number of degrees of freedom per wavelength close to 4.

Sevilla and Huerta [22] showed the importance of good representation of the geometry with NURBS-Enhanced Finite Elements. They developed mapped elements whose approximation is based on classical Finite Element interpolation functions. The mapping is chosen such that the geometry is based on Non-Uniform Rational B-Splines (NURBS). The influence of correct representation of the geometry had already been pointed out by Hughes [26] with isogeometric elements. The use of NURBS has a second advantage which allows to quickly link the CAD model with the mesh. No additional communication is required in the case of mesh refinement.

In this thesis, the Partition of Unity Method is explored. This method has attractive features as it accommodates unstructured meshes, it generates a continuous solution at all points and nodal definition is preserved, leading to a sparse matrix system. As explained in the introduction, the Partition of Unity Method has already been applied to wave prop-

agation with numerical solutions enriched by plane wave functions. This thesis considers a polynomial Partition of Unity Method developed for convected acoustic propagation in cavities or unbounded domains.

2.5 Partition of Unity Method

The Galerkin Method, based on the variational formulation, restricts the solution $\tilde{\phi}_a$ to belong to a subspace $\mathcal{V}^h \subset \mathcal{V}$. The approximated solution $\tilde{\phi}^h$ is built from basis (or interpolation) functions $(\Phi_j(\mathbf{x}), \mathbf{x} \in \mathbb{R}^n)$ and n_u unknown parameters (α_j) :

$$\tilde{\phi}^h(\mathbf{x}) = \sum_{j=1}^{n_u} \Phi_j(\mathbf{x}) \alpha_j \quad (2.46)$$

This choice applied to the variational formulation (2.35), leads to one equation with n_u unknowns (equation 2.47).

$$\begin{aligned} & - \int_{\Omega} \left(\rho_0 \nabla \tilde{\phi}^h - \frac{\rho_0}{c_0^2} (\mathbf{v}_0 \cdot \nabla \tilde{\phi}^h) \mathbf{v}_0 \right) \cdot \nabla W d\Omega \\ & - i\omega \int_{\Omega} \frac{\rho_0}{c_0^2} \left(W \mathbf{v}_0 \cdot \nabla \tilde{\phi}^h - \tilde{\phi}^h \mathbf{v}_0 \cdot \nabla W \right) d\Omega + \omega^2 \int_{\Omega} \frac{\rho_0}{c_0^2} W \tilde{\phi}^h d\Omega \\ & = \int_S \frac{\rho_0}{c_0^2} W \left(\mathbf{v}_0 \cdot \nabla \tilde{\phi}_a \right) \mathbf{n} \cdot \mathbf{v}_0 dS - \int_S \rho_0 W \mathbf{n} \cdot \nabla \tilde{\phi}_a dS \\ & + i\omega \int_S \left(\frac{\rho_0}{c_0^2} W \tilde{\phi}_a \mathbf{v}_0 \cdot \mathbf{n} \right) dS, \quad \forall W \in \mathcal{V} \end{aligned} \quad (2.47)$$

The approximated solution is obtained by choosing n_u number of weight functions W_j constructed in the subspace \mathcal{V}^h and solving the linear system of n_u equations and n_u unknowns. The continuous variational formulation has been transformed to a discrete problem.

The Partition of Unity Method has originally been proposed by Melenk and Babuška [8]. It is a Galerkin method for which the approximation space (\mathcal{V}^h) is based on a partition of the domain Ω and defining the approximation functions on each subdomains.

The domain $\Omega \subset \mathbb{R}^n$ is subdivided in a number of elements (e.g. lines for $\Omega \subset \mathbb{R}^1$; quadrangles and triangles for $\Omega \subset \mathbb{R}^2$; hexahedron and tetrahedron for $\Omega \subset \mathbb{R}^3$). Nodes are created at the vertices of each element. Note that elements sharing a vertex, share the same node.

In the case of Partition of Unity Finite Element Method, subdomains Ω_j are created with the union of elements sharing the node j (of coordinates \mathbf{x}_j). There is the same number of nodes (let say *nodes*) than the number of subdomains.

We define Ω_j as the open cover of Ω satisfying the pointwise overlap condition:

$$\exists M \in \mathbb{N} : \text{card}\{j \mid \mathbf{x} \in \Omega_j\} \leq M \quad \forall \mathbf{x} \in \Omega \quad (2.48)$$

This notation introduced by Melenk and Babuška [8] means that a point \mathbf{x} included in the domain Ω is included in a finite number of open cover Ω_j .

The Partition of Unity function N_j is defined over the subdomain Ω_j such that it satisfies:

$$\begin{cases} \sum_{j=1}^{\text{nodes}} N_j(\mathbf{x}) = 1 & \text{on } \Omega \\ \|N_j\|_{L^\infty(\mathbb{R}^n)} \leq C_\infty \\ \|\nabla N_j\|_{L^\infty(\mathbb{R}^n)} \leq \frac{C_G}{\text{diam}\Omega_j} \end{cases} \quad (2.49)$$

where C_∞ and C_G are constants. These relations have been introduced by Melenk and Babuška [8] to define the Partition of Unity functions properties: these functions and their derivatives are finite and the functions form a partition of unity.

In this work, the Partition of Unity functions are chosen to be the classical hat functions. However, the Partition of Unity functions can be built with Shepard functions (based on rational functions) or piecewise polynomial functions [43]. This allows for the construction of approximations with any desired regularity.

Let the local approximation functions (V_j), also called enrichment functions, be chosen in the local approximation space (\mathcal{V}_j):

$$V_j \in \mathcal{V}_j; \quad \mathcal{V}_j \subset H^1(\Omega_j \cap \Omega) \quad (2.50)$$

where V_j is a combination of functions included in \mathcal{V}_j such that $V_j = \sum_{l=1}^{n(j)} V_{jl} e_{jl}$, with $n(j)$ being the size of the local approximation space, for the node j . It is equivalent to the number of unknowns e_{jl} at the node j . The size of this local space may vary from node to node.

The Partition of Unity space is defined by:

$$\mathcal{V}^h := \sum_{j=1}^{\text{nodes}} N_j \mathcal{V}_j = \left\{ \sum_{j=1}^{\text{nodes}} N_j V_j \mid V_j \in \mathcal{V}_j \right\} \subset H^1(\Omega) \quad (2.51)$$

The approximated acoustic potential is given by:

$$\begin{aligned}
\tilde{\phi}^h &= \sum_{j=1}^{nodes} N_j V_j \in \mathcal{V}^h \subset H^1(\Omega) \\
&= \sum_{j=1}^{nodes} N_j \sum_{l=1}^{n(j)} V_{jl} e_{jl} \\
&= \sum_{j=1}^{nodes} \sum_{l=1}^{n(j)} N_j V_{jl} e_{jl} \\
&= \sum_{\alpha^h=1}^{n_u} \Phi_\alpha e_\alpha \\
&= \{\mathbf{\Phi}\}^t \{\phi_a\}
\end{aligned} \tag{2.52}$$

where $\{\phi_a\}$ corresponds to the unknowns e_{jl} such that they are written in a vector and n_u is the number of degrees of freedom, the size of the vector $\{\phi_a\}$. The Partition of Unity shape functions $\Phi_\alpha = N_j V_{jl}$ are also written in a vector $\{\mathbf{\Phi}\}$.

We choose the weight functions W_α to be the complex conjugate of the shape functions Φ_α , following a Petrov-Galerkin approach. This leads to the vector $\{\mathbf{W}\} = \{\mathbf{\Phi}\}^*$.

The matrix form of the convected wave variational formulation is given hereafter:

$$([\mathbf{K}] + i\omega [\mathbf{C}] - \omega^2 [\mathbf{M}]) \{\phi_a\} = \{\mathbf{F}\} \tag{2.53}$$

$$K_{\alpha\beta} = - \int_{\Omega} \left(\rho_0 \nabla \Phi_\beta - \frac{\rho_0}{c_0^2} (\mathbf{v}_0 \cdot \nabla \Phi_\beta) \mathbf{v}_0 \right) \cdot \nabla W_\alpha d\Omega \tag{2.54}$$

$$C_{\alpha\beta} = - \int_{\Omega} \frac{\rho_0}{c_0^2} (W_\alpha \mathbf{v}_0 \cdot \nabla \Phi_\beta - \Phi_\beta \mathbf{v}_0 \cdot \nabla W_\alpha) d\Omega \tag{2.55}$$

$$M_{\alpha\beta} = - \int_{\Omega} \frac{\rho_0}{c_0^2} W_\alpha \Phi_\beta d\Omega \tag{2.56}$$

$$\begin{aligned}
F_\alpha &= \int_S \frac{\rho_0}{c_0^2} W_\alpha (\mathbf{v}_0 \cdot \nabla \tilde{\phi}_a) \mathbf{n} \cdot \mathbf{v}_0 dS - \int_S \rho_0 W_\alpha \mathbf{n} \cdot \nabla \tilde{\phi}_a dS \\
&\quad + i\omega \int_S \left(\frac{\rho_0}{c_0^2} W_\alpha \tilde{\phi}_a \mathbf{v}_0 \cdot \mathbf{n} \right) dS
\end{aligned} \tag{2.57}$$

The advantages of the Partition of Unity Method are the following:

- It accommodates unstructured meshes.
- It generates a continuous solution at all points.
- It preserves nodal definition, leading to a sparse matrix system.
- It permits to add a priori knowledge about the differential equation in the local approximation space (e.g.: plane waves, see [28, 9]).
- It allows to choose an appropriate local approximation space separately for each subdomain Ω_i
- It may be used to construct approximation spaces of desired regularity.

In the following, we restrict the Partition of Unity functions N_j to be bilinear functions defined over the subdomain Ω_j . N_j takes the unity value at the node \mathbf{x}_j and is equal to zero at the other nodes of the subdomain. We also focus on local approximation spaces \mathcal{V}^h which are composed of polynomial functions.

The integration is performed numerically by the use of the Gauss-Legendre integration scheme since the integrands are polynomials. The number of Gauss points NG used for the numerical integration of a polynomial of order p follows at least the rule of exact integration: $NG = (p + 1) / 2$.

We decided not to focus on local approximation spaces constructed with plane waves (e.g. $e^{i\mathbf{k}\mathbf{x}}$) or trigonometric functions (e.g. $\cos \mathbf{k}\mathbf{x}$, $\sin \mathbf{k}\mathbf{x}$), as it has been done for instance by Lacroix [68], Debel [24], Gamallo [28], Laghrouche [9] and others, for several reasons:

1. The variational formulation leads to the matrix form given at equation 2.53, whatever is the local approximation space. When harmonic functions are used, the matrices become frequency dependent as the excitation frequency appears in the shape and weight functions. The matrices ($\mathbf{K}(\omega)$, $\mathbf{C}(\omega)$, $\mathbf{M}(\omega)$) have to be built for each frequency that have to be taken into account for the application.

This is not the case for polynomial functions which lead to non frequency dependent matrices. In this case, the computation of the acoustic potential at several frequencies can be obtained by solving the system 2.53 without reconstructing the matrices.

2. Since we deal with non-uniform flow, the set of plane waves in the local approximation space \mathcal{V}_j has to take into account the local mean flow velocity at the node j (e.g. in two-dimension, for a flow along x axis, θ being the direction of the plane wave and $M_{0,j}$ the mean Mach number at the node j : $e^{-ik\left(\frac{\cos(x)}{1-M_{0,j}\cos(\theta)} + \frac{\sin(y)}{1-M_{0,j}\cos(\theta)}\right)}$). This means that the size of the mesh does not only depend on the quality of the local approximation but also on the variation of the flow velocity. The mesh therefore depends on the acoustic resolution but also on the spatial variation of the mean flow velocity. An application

with a large spatial variations of mean flow velocity would require a dense mesh with highly oscillating functions to integrate.

3. This choice of enrichment functions requires a large number of integration points for the numerical Gauss-Legendre integration. The numerical Gauss-Legendre integration is, indeed, not appropriate to the integration of harmonic functions as it has been designed to exactly evaluate the integral of polynomial functions (the integration of a one-dimensional polynomial function of order p requires $NG = \frac{p+1}{2}$ Gauss integration points, or NG^n for $\mathbf{x} \in \mathbb{R}^n$). The integration of a harmonic function with NG Gauss points with this technique is equivalent to the integration of a polynomial function of order $2NG - 1$. This explains the reason why the integration of harmonic functions requires a high number of integration points if the Gauss-Legendre integration is used instead of another technique more suitable to harmonic integration. To illustrate this remark, note that Laghrouche [9] used 120*120 Gauss points per elements for simulating a two-dimensional radiating cylinder with $ka = 10\pi$ (a being the radius of the cylinder). The size of the elements is such that an element contains 10 wavelength in the radial direction and up to 12 in the angular direction. This gets worse for higher excitation frequencies.

The numerical integration of the matrices considering a local harmonic basis is the topic of current researches. Semi-analytical rules have been proposed [53] for straight edge finite elements (two-dimensional quadrangle and triangle elements). Recently, Gabard [88] defined exact integration of polynomial-exponential products for arbitrary polygons in two dimensions and for arbitrary polygonal surfaces or polyhedral volumes in three dimensions. These exact solutions require a limited number of operations and the computational cost is independent of the wavenumber used in the integral.

Let us consider, for instance, the following second order polynomial enrichment 2.58, in one-, two- or three dimensions, leading to respectively, 3, 6 or 10 functions in the local approximation space. The creation of a shape function $N_j V_{jl}$ is illustrated for the one- and two-dimensional cases in figures 2.2 and 2.3, respectively.

$$\begin{aligned} V &= \{1, x, x^2\} \quad \text{in } \mathbb{R}^1 \\ V &= \{1, x, y, x^2, y^2, xy\} \quad \text{in } \mathbb{R}^2 \\ V &= \{1, x, y, z, x^2, y^2, z^2, xy, xz, yz\} \quad \text{in } \mathbb{R}^3 \end{aligned} \quad (2.58)$$

The same local approximation space can be prescribed to all the subdomains Ω_i or this local approximation space can be defined from node to node, depending on the spatial complexity of the local potential variation (e.g. high mach number, sharp geometry,...).

For the three-dimensional simulation, we developed a hexahedral mapped element with 8 nodes and 12 additional mapping points (figure 2.4). The nodes are located at the vertices of the element, while the mapping points stand along the edges of the element. Global and local coordinates are linked by the following mapping, where the mapping functions M_i are given in appendix 10.1.

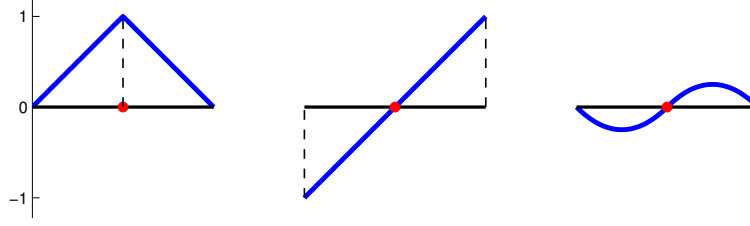


Fig. 2.2. Construction of the approximation: illustration for the node j (located at the center of the subdomain Ω_j which corresponds to the two elements) of the Partition of Unity function $N_j(\mathbf{x})$ (left), the enrichment function $V_{jl}(\mathbf{x})$ (center) and the shape function $\phi_{jl} = N_j(\mathbf{x})V_{jl}(\mathbf{x})$ (right) with an enrichment $V_{jl}(\mathbf{x}) = \frac{(x-x_j)}{h_x}$ where h_x is the highest distance between the node j and any point in its subdomain Ω_j in the $\mathbf{1}_x$ direction.

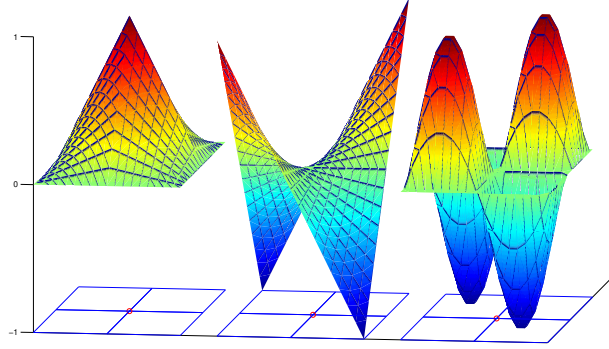


Fig. 2.3. Construction of the approximation: illustration for the node j (located at the center of the subdomain Ω_j which corresponds to the four elements) of the Partition of Unity function $N_j(\mathbf{x})$ (left), the enrichment function $V_{jl}(\mathbf{x})$ (center) and the shape function $\phi_{jl} = N_j(\mathbf{x})V_{jl}(\mathbf{x})$ (right) with an enrichment $V_{jl}(\mathbf{x}) = \frac{(x-x_j)(y-y_j)}{h_x h_y}$ where (h_x, h_y) are the highest distances between the node j and any point in its subdomain Ω_j , respectively in the $\mathbf{1}_x$ and $\mathbf{1}_y$ directions. Note that in this case, the shape function has been normalized.

$$\begin{cases} x = \sum_{i=1}^{20} M_i(\xi, \eta, \zeta) x_i \\ y = \sum_{i=1}^{20} M_i(\xi, \eta, \zeta) y_i \\ z = \sum_{i=1}^{20} M_i(\xi, \eta, \zeta) z_i \end{cases} \quad (2.59)$$

The geometry is constructed with all of the 20 nodes and points while the Partition of Unity functions and the local approximation functions are defined only at nodes. The aim of the 12 additional mapping points is to allow the element to have curved edges (or non-planar faces). The representation of the exact geometry of the application with the mesh is an important feature to obtain accurate numerical results (as we observed in [69]). The lack of approximation of the geometry is a limiting factor for the numerical solution [26]: ‘Then use of a fixed polynomial approximation to geometry has been shown by Szabó et al. [27] to be limiting. As solution polynomial order is increased, the error plateaus at some level and cannot be further reduced.’

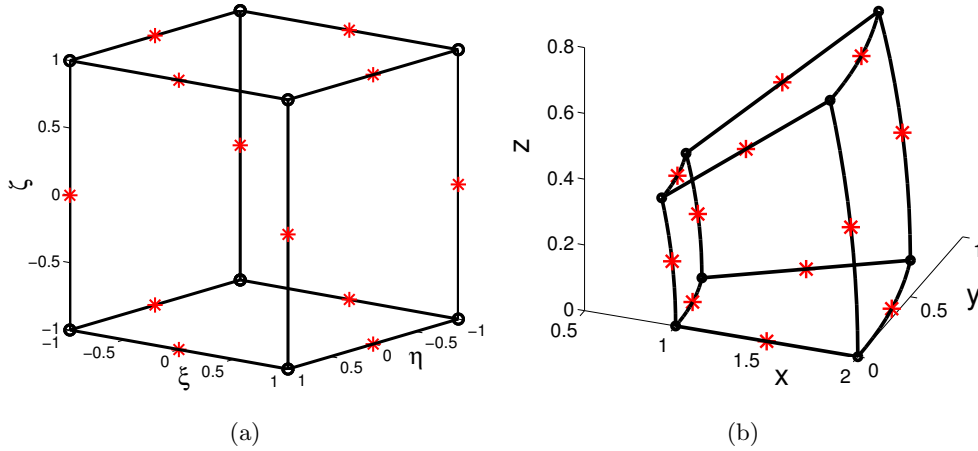


Fig. 2.4. View of an element in its local (ξ, η, ζ) (a) and global (x, y, z) (b) coordinates. The 8 circles correspond to the nodes and the stars represent the 12 mapping points.

Note that classical linear finite element results can be obtained by a particular version of the Partition of Unity Method. This is called ‘*degenerated*’ Partition of Unity Method. Indeed, if the enrichment functions for all the nodes are constant and equal to $\{1\}$, the approximation becomes:

$$\tilde{\phi}^h = \sum_{j=1}^{nodes} N_j(\mathbf{x}) e_{j1} \quad (2.60)$$

2.6 Modal and transmitted boundary conditions

The acoustic field in an infinite or semi-infinite hard-walled duct with uniform flow along the duct axis can be expressed as a combination of fundamental solutions, called acoustic modes [42]. The conditions at the inlet or exhaust plane of a duct can therefore often be represented by a modal boundary condition (fig. 2.5). This is particularly useful in application to mufflers, HVAC systems, and turbofan intake or by-pass ducts, since it permits a ‘source’ to be defined explicitly in terms of the amplitudes of the incident modes. It also permits the specification of an exact anechoic termination when the amplitudes of all reflected modes are set to zero.

2.6.1 Propagation in a straight duct

Consider the case of a straight duct with arbitrary cross section where the mean flow in the duct is uniform and oriented with the duct axis (let say z). We will restrict our study

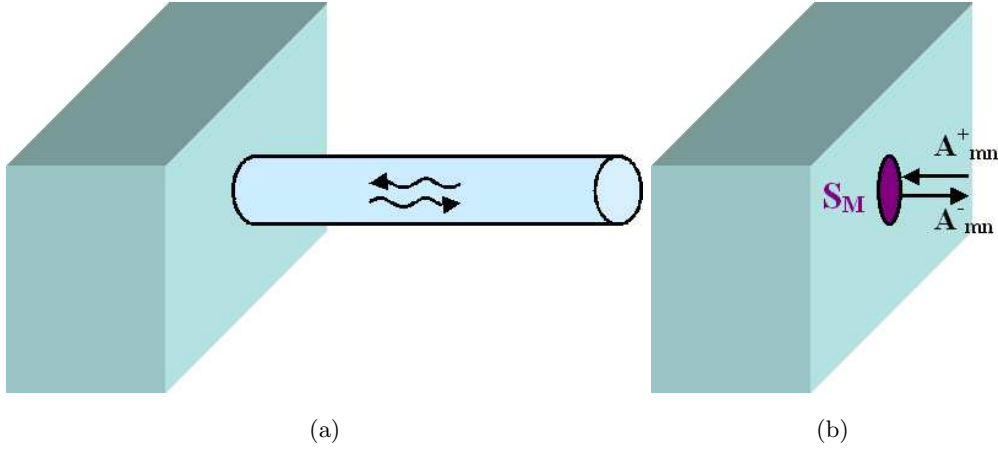


Fig. 2.5. An application with a cylindrical duct radiating in a box (a). The cylindrical duct is replaced by a modal boundary condition on the surface S_M (b) such that the computational domain to be considered is the box only

to hard-walled axisymmetric ducts, but the same developments can be performed for lined ducts (see appendix 10.2) or other cross sections, i.e. rectangular [44] or arbitrary ones [54].

Wave propagation in an infinite axisymmetric duct can be decomposed in a series of right and left traveling modes:

$$\tilde{\phi}_a = \sum_{m=-\infty}^{\infty} \sum_{n=0}^{\infty} \left(A_{mn}^+ E_{mn}^+ e^{-im\theta} e^{-iK_{z,mn}^+ z} + A_{mn}^- E_{mn}^- e^{-im\theta} e^{-iK_{z,mn}^- z} \right) \quad (2.61)$$

where (r, θ, z) are the cylindrical coordinates of the axisymmetric duct, (m, n) are respectively the angular and radial mode numbers, A_{mn}^{\pm} are complex amplitudes of the right and left traveling modes (E_{mn}^{\pm}) and $K_{z,mn}^{\pm}$ their corresponding axial wavenumbers.

The modes and wavenumbers are obtained by solving the convected wave equation 2.32 in a duct with uniform mean flow along the axial direction, by considering separation of variables and appropriate boundary conditions.

The modified convected wave equation in cylindrical coordinates for uniform mean flow ($\mathbf{v}_0 = v_0 \mathbf{1}_z$) is:

$$\frac{\partial^2 \tilde{\phi}_a}{\partial r^2} + \frac{1}{r} \frac{\partial \tilde{\phi}_a}{\partial r} + \frac{1}{r^2} \frac{\partial^2 \tilde{\phi}_a}{\partial \theta^2} + (1 - M_0^2) \frac{\partial^2 \tilde{\phi}_a}{\partial z^2} - 2ikM_0 \frac{\partial \tilde{\phi}_a}{\partial z} + k^2 \tilde{\phi}_a = 0 \quad (2.62)$$

where $M_0 = v_0/c_0$ is the Mach number in the duct and $k = \omega/c_0$ is the wavenumber.

The solution is assumed to have the following form:

$$\tilde{\phi}_a = \phi_r \phi_z e^{-im\theta} \quad (2.63)$$

This leads to a system of two equations (2.64, 2.65) where $k_{r,mn}$ is the radial wavenumber such that $k^2 = k_{z,mn}^2 + k_{r,mn}^2$:

$$\frac{\partial^2 \phi_r}{\partial r^2} + \frac{1}{r} \frac{\partial \phi_r}{\partial r} + \left(k_{r,mn}^2 - \frac{m^2}{r^2} \right) \phi_r = 0 \quad (2.64)$$

$$(1 - M_0^2) \frac{\partial^2 \phi_z}{\partial z^2} - 2ikM_0 \frac{\partial \phi_z}{\partial z} + k_{z,mn}^2 \phi_z = 0 \quad (2.65)$$

Equation 2.64 can be rewritten as:

$$r^2 \frac{\partial^2 \phi_r}{\partial r^2} + r \frac{\partial \phi_r}{\partial r} + (k_{r,mn}^2 r^2 - m^2) \phi_r = 0 \quad (2.66)$$

where solutions are given by Bessel functions of the first or the second kind, respectively $J_m(k_{r,mn}r)$ and $Y_m(k_{r,mn}r)$.

Equation 2.65 can be solved by looking for a solution of the following form $\phi_z = Ae^{gz}$. Equation 2.65 becomes:

$$\beta^2 g^2 - 2ikM_0 g + k_{z,mn}^2 = 0 \quad (2.67)$$

with $\beta = \sqrt{1 - M_0^2}$, or,

$$g = -i \frac{-kM_0 \mp \sqrt{k^2 M_0^2 + k_{z,mn}^2 \beta^2}}{\beta^2}$$

$$g = -i \frac{-kM_0 \mp \sqrt{k^2 - k_{r,mn}^2 \beta^2}}{\beta^2} \quad (2.68)$$

It follows that wave propagation in axisymmetric ducts is:

$$\tilde{\phi}_a = \sum_{m=-\infty}^{\infty} \sum_{n=0}^{\infty} \left(A_{mn}^+ E_{mn}^+ e^{-iK_{z,mn}^+ z} + A_{mn}^- E_{mn}^- e^{-iK_{z,mn}^- z} \right) e^{-im\theta} \quad (2.69)$$

$$E_{mn}^{\pm} = (AJ_m(k_{r,mn}^{\pm}r) + BY_m(k_{r,mn}^{\pm}r)) \quad (2.70)$$

$$K_{z,mn}^{\pm} = \frac{-kM_0 \mp \sqrt{k^2 - k_{r,mn}^2 \beta^2}}{\beta^2} \quad (2.71)$$

The radial wavenumbers and modes are obtained by considering appropriate cross section and boundary conditions. In the case of a hard walled duct, the displacement of the wall is null $\tilde{u}_n = 0$ and the normal component of the acoustic particle velocity $\tilde{\mathbf{v}}_a \cdot \mathbf{n}$ or $\nabla \tilde{\phi}_a \cdot \mathbf{n} = 0$ at the walls.

Note that the expression of the potential in the duct (equation 2.69) corresponds to an infinite series but it can be truncated. As soon as the radial wavenumber is greater than k/β , the square root in the expression of $K_{z,mn}^{\pm}$ becomes complex instead of purely

real. This means that $e^{-iK_{z,mn}^\pm z}$ corresponds to an exponentially decaying wave, as steep as the imaginary part is big. The mode is said to be evanescent. Propagating and evanescent modes are also known as cut-on and cut-off modes.

The potential can be computed with all the propagating and a few evanescent modes. This allows us to truncate the infinite series.

Hard walled duct with a circular cross section

In the case of a cylindrical duct with a circular cross section of radius R , the hard wall boundary condition becomes $\left. \frac{\partial \tilde{\phi}_a}{\partial r} \right|_{r=R} = 0$. Radial modes 2.70 are Bessel functions of the first kind. Those of the second kind have to be rejected as they are singular at the origin ($r = 0$). This corresponds to $A = 1$ and $B = 0$.

The radial wavenumbers propagating in the duct are obtained by solving:

$$J'_m(k_{r,mn}^\pm r) \Big|_{r=R} = 0 \quad (2.72)$$

or, using well known mathematical relations:

$$\begin{aligned} J_{m-1}(X) \Big|_{r=R} - \frac{m}{X} J_m(X) \Big|_{r=R} &= 0 \\ X &= k_{r,mn}^\pm r \end{aligned} \quad (2.73)$$

Note that the right and left propagating radial wavenumbers $k_{r,mn}^\pm$ are equal in the case of hard-walled circular duct with uniform mean flow.

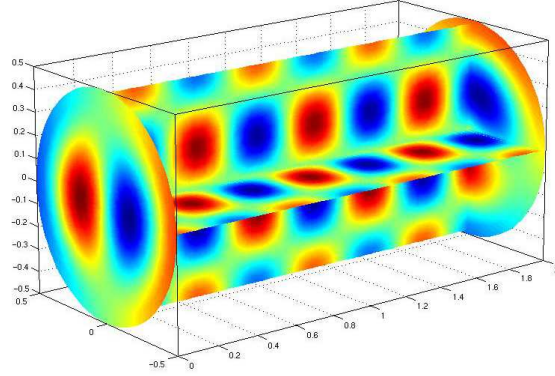
The propagation of a mode is illustrated in figure 2.6 in a cylindrical duct (circular cross-section) with and without uniform mean flow.

Hard walled duct with an annular cross section

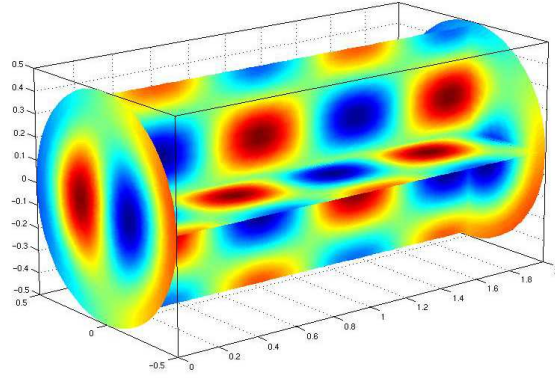
The cross section of the duct is composed by two circular walls, R_i and R_o being respectively the inner and outer radius. Since both surfaces are assumed to be hard walled, the derivative of the potential has to vanish for $r = R_i$ and $r = R_o$. There is no difference between $k_{r,mn}^+$ and $k_{r,mn}^-$. This leads to a system of two equations:

$$\begin{bmatrix} J'_m(k_{r,mn} R_i) & Y'_m(k_{r,mn} R_i) \\ J'_m(k_{r,mn} R_o) & Y'_m(k_{r,mn} R_o) \end{bmatrix} \begin{Bmatrix} A \\ B \end{Bmatrix} = \begin{Bmatrix} 0 \\ 0 \end{Bmatrix} \quad (2.74)$$

The determinant of the matrix has to be equal to zero if solutions different from the trivial $A = B = 0$ are sought.



(a)



(b)

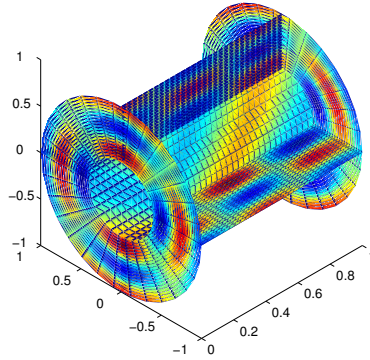
Fig. 2.6. Three-dimensional pressure distribution for wave propagation in a hard-walled circular duct ($R = 0.5m$) at 800 Hz ($kR = 7.39$): the figures represent the propagation (real part of the pressure) of the second radial mode, first azimuthal order ($m = 1, n = 2$) with zero mean flow (a) and with a mean flow velocity of 160m/s in the x direction (b).

Roots of equation 2.75 give the radial wavenumbers:

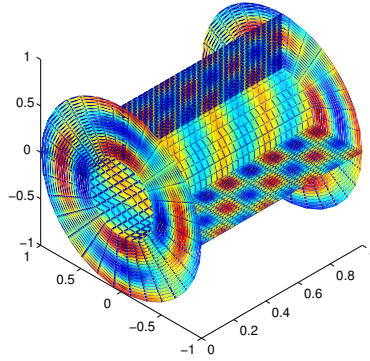
$$J'_m(k_{r,mn}R_i)Y'_m(k_{r,mn}R_o) - J'_m(k_{r,mn}R_o)Y'_m(k_{r,mn}R_i) = 0 \quad (2.75)$$

If A is chosen equal to 1, we can determine the value of B by using the first equation of system 2.74. The propagation in an annular duct is then given by the following decomposition:

$$\begin{aligned} \tilde{\phi}_a = \sum_{m=-\infty}^{\infty} \sum_{n=0}^{\infty} & \left(A_{mn}^+ e^{-iK_{z,mn}^+ z} + A_{mn}^- e^{-iK_{z,mn}^- z} \right) e^{-im\theta} \\ & \left(J_m(k_{r,mn}r) - \frac{J'_m(k_{r,mn}R_i)}{Y'_m(k_{r,mn}R_i)} Y_m(k_{r,mn}r) \right) \end{aligned} \quad (2.76)$$



(a)



(b)

Fig. 2.7. Three-dimensional pressure distribution for wave propagation in a hard-walled annular duct ($r_i = 0.4m, r_o = 1m$) at 800 Hz ($kR = 7.39$) : the figures represent the propagation (real part of the pressure) of the second radial mode, second azimuthal order ($m = 2, n = 2$) with zero mean flow (a) and with a mean flow velocity of 160m/s opposite to the wave direction (b).

The propagation of a mode is illustrated in figure 2.7 in a cylindrical duct (annular cross-section) with and without uniform mean flow.

Energy

In practical applications such as turbofan radiation, the acoustic source is prescribed by given modal intensities instead of modal amplitudes. Sound intensity \mathbf{I} [52] is a vector quantity and defined as the time average of the net flow of sound energy through a unit area in a direction perpendicular to the area.

In the special case of convected wave propagation in a non-uniform irrotational mean flow free from entropy variations, the expression of the time average energy flow out of a

surface S_M is given by Morfey [56]:

$$\langle E \rangle = \int_{S_M} \langle J' m'_i \rangle dS_i \quad (2.77)$$

$$\langle J' m'_i \rangle = \langle p_a v_{a,i} \rangle + \frac{v_{0,i}}{\rho_0 c_0^2} \langle p_a^2 \rangle + \frac{v_{0,i} v_{0,j}}{\rho_0 c_0^2} \langle p_a v_{a,j} \rangle + \rho_0 v_{0,j} \langle v_{a,i} v_{a,j} \rangle \quad (2.78)$$

where J' and m'_i are the stagnation entropy ($J = h + v^2/2$) and the mass flux ($m_i = \rho_0 v_i$), both estimated to first order. $p_a(\mathbf{x}, t)$ and $\mathbf{v}_a(\mathbf{x}, t)$ are instantaneous acoustic pressure and velocity.

In the case of the wave propagation in a duct, the mean flow is oriented along the duct axis ($\mathbf{v}_0 = v_{0,z} \mathbf{1}_z$). The component, along the duct axis, of the sound intensity I over the modal boundary S_M is given at equation 2.79 (A being the area of the cross-section).

$$\langle I \rangle = \frac{1}{A} \int_{S_M} \Re(\tilde{p}_a \tilde{v}_{a,z}^*) (1 + M_0^2) + M_0 \left(\frac{\tilde{p}_a \tilde{p}_a^*}{\rho_0 c_0} + \rho_0 c_0 \tilde{v}_{a,z} \tilde{v}_{a,z}^* \right) dS \quad (2.79)$$

In the case of cylindrical ducts, the acoustic pressure $\tilde{p}_{a,mn}$ and velocity $\tilde{v}_{a,z,mn}$ related to the mn^{th} mode are given by the set of relations 2.80.

$$\begin{aligned} \tilde{p}_{a,mn} &= -\rho_0 c_0 \left(ik \tilde{\phi}_{a,mn} + M_0 \frac{\partial \tilde{\phi}_{a,mn}}{\partial z} \right) \\ \tilde{\phi}_{a,mn}^+ &= A_{mn}^+ E_{mn}^+ e^{-im\theta} e^{-iK_{z,mn}^+ z} \\ \tilde{p}_{a,mn}|_{S_M} &= -i\rho_0 c_0 A_{mn}^+ E_{mn}^+ e^{-im\theta} (k - K_{z,mn}^+ M_0) \\ \tilde{v}_{a,z,mn} &= \frac{\partial \tilde{\phi}_{a,mn}^+}{\partial z} \\ \tilde{v}_{a,z,mn}|_{S_M} &= -iK_{z,mn}^+ A_{mn}^+ E_{mn}^+ e^{-im\theta} \end{aligned} \quad (2.80)$$

Substitution of expressions 2.80 into equation 2.79 gives the sound intensity I_{mn} of the mn^{th} mode:

$$\begin{aligned} I_{mn}^+ &= \left((1 + M_0^2) k \Re(K_{z,mn}^+) + M_0 |k - M_0 K_{z,mn}^+|^2 - M_0^3 |K_{z,mn}^+|^2 \right) \\ &\quad \frac{\rho_0 c_0 |A_{mn}^+|^2}{2A} \int_{S_M} E_{mn}^+ dS \end{aligned} \quad (2.81)$$

In the particular case of a circular cross-section of radius R , the integral of the radial mode over the modal boundary is:

$$\int_{S_M} J_m^2(k_{r,mn} r) dS = \pi \left(R^2 - \frac{m^2}{k_{r,mn}^2} \right) J_m^2(k_{r,mn} R) \quad (2.82)$$

Equation 2.81 links the incident amplitude (A_{mn}^+) of mode (m, n) to the incident intensity (I_{mn}^+) of the related mode. It is possible to prescribe a mode of known intensity.

2.6.2 Modal coupling

The axial z axis in the duct cylindrical coordinates is considered, in the present dissertation, to be aligned with the x axis of the computational domain (figure 2.8). As the flow in the duct is uniform and oriented with the axial direction, the flow on the boundary S_M is also considered as being uniform : $\mathbf{v}_0 = v_0 \mathbf{1}_x$ and its Mach number $M_0 = v_0/c_0$. The definition of F_α defined by expression 2.57 is then reduced, on the boundary S_M , to:

$$F_\alpha = \int_{S_M} \rho_0 W_\alpha \left(\beta^2 \frac{\partial \tilde{\phi}_a}{\partial x} - i M_0 k \tilde{\phi}_a \right) dS \quad (2.83)$$

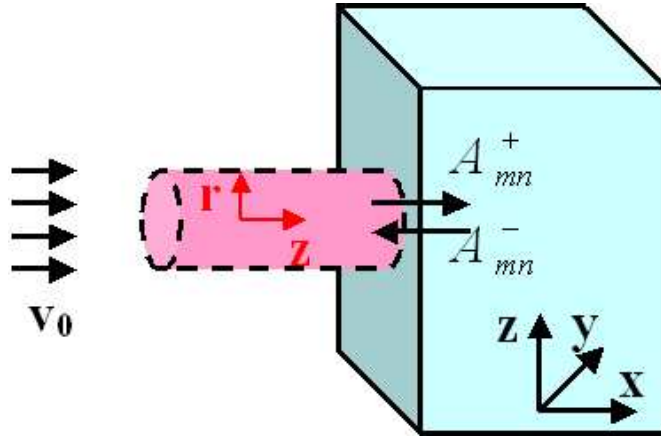


Fig. 2.8. Computational domain (in blue) with its coordinate system (x, y, z) and the duct (in pink, (z, r, θ)) which will be replaced by a modal boundary condition by prescribing incident and reflected modes, (A_{mn}^+, A_{mn}^-) respectively.

The modal boundary condition is based on the previous decomposition of the potential in the duct. We replace the expression of the potential in equation 2.83 by the truncated series representing the propagation in the duct at the modal boundary S_M . Note that in the duct coordinates, z is constant on S_M , e.g. if on S_M the cylindrical coordinates of the duct are taken such as $z|_{S_M} = 0$ then $e^{-iK_{z,mn}^\pm z} = 1$.

$$\tilde{\phi}_a \Big|_{S_M} = \sum_{m=-N_m}^{N_m} \sum_{n=0}^{N_n} (A_{mn}^+ E_{mn}^+ + A_{mn}^- E_{mn}^-) e^{-im\theta} \quad (2.84)$$

$$\frac{\partial \tilde{\phi}_a}{\partial z} \Big|_{S_M} = \sum_{m=-N_m}^{N_m} \sum_{n=0}^{N_n} (-iK_{z,mn}^+ A_{mn}^+ E_{mn}^+ - iK_{z,mn}^- A_{mn}^- E_{mn}^-) e^{-im\theta} \quad (2.85)$$

where A_{mn}^+ and A_{mn}^- are respectively incident (known) and reflected (unknown) amplitudes, and E_{mn}^\pm are radial modes (depending on the cross section of the duct and the treatment

of the walls). Note that the incident and reflected radial modes E_{mn}^\pm are often identical because the right and left traveling radial wavenumbers are equal excepted for a lined duct with non-zero uniform mean flow (see appendix 10.2).

The system matrix 2.53 becomes underdetermined. It possesses a set of n_u equations and $(n_u + N_M)$ unknowns, where n_u is the number of degrees of freedom and N_M the number of reflected modes. N_M equations have to be added to the system. These additional equations (2.86) are N_M weighted integrals of equation 2.84 where the potential $\tilde{\phi}_a$ is replaced by its numerical approximation $\tilde{\phi}^h$ (equation 2.52).

$$\begin{aligned} & \int_{S_M} W_{M,m'n'} \tilde{\phi}^h dS \\ & = \\ & \int_{S_M} W_{M,m'n'} \left(\sum_{m=-N_m}^{N_m} \sum_{n=0}^{N_n} (A_{mn}^+ E_{mn}^+ + A_{mn}^- E_{mn}^-) e^{-im\theta} \right) dS \end{aligned} \quad (2.86)$$

where $W_{M,m'n'}$ is the weight function for the n^{th} radial mode of the m^{th} azimuthal order is given by expression 2.87.

$$W_{M,m'n'} = i\rho_0 E_{m'n'}^- e^{im'\theta} (\beta^2 K_{z,m'n'}^- + M_0 k) \quad (2.87)$$

Note that the circumferential variation of the weight function is taken to be $e^{im'\theta}$ instead of $e^{-im\theta}$. This has been done to avoid terms like $e^{-2im\theta}$ which would have given zero terms on the diagonal of the ‘modal’ matrices.

The unknown amplitudes of the reflected modes (A_{mn}^-) are sorted such as they can be arranged in a vector $\{\mathbf{a}_M\}$. The same arrangement is applied to radial modes which are sorted with a single index, e.g. E_α^- . Therefore the N_M weight functions $W_{M,m'n'}$ can also be written with a single index: $W_{M,\alpha}$, such that:

$$\sum_{m=-N_m}^{N_m} \sum_{n=0}^{N_n} (A_{mn}^- E_{mn}^- e^{-im\theta}) = \sum_{\gamma=1}^{N_M} (a_{M,\gamma} E_\gamma^- e^{-im_\gamma\theta}) \quad (2.88)$$

where m_γ is the angular mode m for the index γ .

This vector of reflected modal amplitude is then included in front of the vector of unknowns of the computational domain $\{\phi_a\}$. This leads to the following matrix system:

$$\begin{bmatrix} [\mathbf{D}_M] & [\mathbf{C}_M] \\ [\mathbf{A}_M] & ([\mathbf{K}] + i\omega [\mathbf{C}] - \omega^2 [\mathbf{M}]) \end{bmatrix} \begin{Bmatrix} \{\mathbf{a}_M\} \\ \{\phi_a\} \end{Bmatrix} = \begin{Bmatrix} \{\mathbf{E}_M\} \\ \{\mathbf{B}_M\} \end{Bmatrix} + \begin{Bmatrix} \{\mathbf{0}\} \\ \{\mathbf{F}\} \end{Bmatrix} \quad (2.89)$$

where $\{\mathbf{F}\}$ corresponds to the contribution of all solicitations excepted the modal boundary condition.

The matrices coming from the modal boundary conditions are:

$$A_{M,\alpha\gamma} = i\rho_0 (\beta^2 K_{z,\gamma}^- + M_0 k) \int_{S_M} W_\alpha E_\gamma^- e^{-im_\gamma\theta} dS \quad (2.90)$$

$$B_{M,\alpha} = -i\rho_0 \sum_{a=1}^{N_M} A_a^+ (\beta^2 K_{z,a}^+ + M_0 k) \int_{S_M} W_\alpha E_a^+ e^{-im_a\theta} dS \quad (2.91)$$

$$C_{M,\alpha\gamma} = i\rho_0 (\beta^2 K_{z,\alpha}^- + M_0 k) \int_{S_M} \Phi_\gamma E_\alpha^- e^{im_\alpha\theta} dS \quad (2.92)$$

$$D_{M,\alpha\gamma} = -i\rho_0 (\beta^2 K_{z,\alpha}^- + M_0 k) \int_{S_M} E_\alpha^- e^{im_\alpha\theta} E_\gamma^- e^{-im_\gamma\theta} dS \quad (2.93)$$

$$E_{M,\alpha} = i\rho_0 (\beta^2 K_{z,\alpha}^- + M_0 k) \sum_{a=1}^{N_M} A_a^+ \int_{S_M} E_a^+ e^{-im_a\theta} E_\alpha^- e^{im_\alpha\theta} dS \quad (2.94)$$

where \mathbf{W} and Φ are the Partition of Unity shape functions (equation 2.52). \mathbf{D} is diagonal for all cross sections as radial modes are Bessels functions which are orthogonal¹. Matrices \mathbf{A}_M , \mathbf{C}_M , \mathbf{D}_M are respectively of size $(n_u \times N_M)$, $(N_M \times n_u)$ and $(N_M \times N_M)$, while vectors \mathbf{B}_M and \mathbf{E}_M have the following sizes: $(n_u \times 1)$ and $(N_M \times 1)$.

Transmitted boundary conditions can be treated as modal boundary conditions excepted that all incident amplitudes are nulls. This means that we only consider the anechoic termination allowing reflected modes to penetrate in the duct but that there is no noise coming from the duct towards the computational domain.

2.7 Unbounded applications: state of the art

Since the current model must also be able to simulate exterior domains, a far field numerical treatment is required which is able to represent an anechoic termination in the presence of mean flow. There exist four families of techniques to simulate acoustic propagation in an unbounded domain (a good overview of recent techniques is given in [57] and its references): the Boundary Element Method (BEM), the Finite Element Method coupled to Non-Reflecting Boundary Conditions (NRBC) prescribed on a truncated domain - the Perfectly Matched Layers (PML) or local/global absorbing boundary conditions (ABC) - and to Infinite Elements.

The Boundary Element Method [58] allows to compute wave propagation in a domain $\Omega \in \mathbb{R}^n$ by discretizing its boundary $S \in \mathbb{R}^{n-1}$. However, this method results in fully populated matrices. This is not convenient to solve the computational system (compared to sparse matrices for the Finite Element Method). Studies showed that the Finite Element

¹ Modal eigen functions are orthogonal for all cross sections not only for cylindrical ones, provided that the walls of the duct are rigid.

Method is more cost-effective for exterior Helmholtz problems, considering the test cases they report (see [33] and its references).

In the case of Non-Reflecting Boundary Conditions, the unbounded domain is truncated and appropriate boundary conditions are applied to eliminate reflected waves on the truncated boundary. These conditions may be based on absorbing (PML) or radiation conditions (ABC).

The Perfectly Matched Layers proposed by Bérenger [59] is a popular method because of its performances, the conceptual simplicity and the ease of implementation. The general principles of the method consist in truncating the infinite domain, then surrounding the truncated domain with a computational layer within the wave is considered as being evanescent, i.e. the propagation possesses an exponential decay such as the waves vanish before they get reflected in the computational domain. Note that a rapid decay corresponds to strong gradients. Special care has then to be taken to avoid spurious reflections at the truncated boundary, see for instance the influence of *hp*-adaptivity on the performance of Perfectly Matched Layers [60].

Absorbing Boundary Conditions is based on radiation conditions. The infinite domain is truncated. An appropriate boundary condition is prescribed on the truncated surface. These conditions may be global (exact) such as the Dirichlet-to-Neumann (DtN) condition. An infinite Fourier series represents the solution in the exterior region. This treatment leads to high accuracy but dense blocks to include in sparse matrices. Another drawback of the Dirichlet-to-Neumann condition corresponds to the geometry of truncated boundaries which is limited to simple shapes, e.g. circle or sphere.

Local Absorbing Boundary Conditions preserve the sparsity of the problem and allow for complex shapes of the truncated boundaries. These local Absorbing Boundary Conditions approximate the Sommerfeld radiation condition on the truncated boundary. Higher order conditions are preferable to lower ones since they allow for a smaller computational truncated region. Since the early 1970s, Bayliss and Turkel [61] proposed a condition based on n hierarchy operators that successively annihilates the first n terms of the far field expansion of Wilcox-Atkinson (equation 2.97), Engquist and Majda [62] based their method on the theory of pseudo-differential operators and Feng [63] proposed the truncation of the asymptotic expansion of the Dirichlet-to-Neumann condition. More recently, high-order boundary conditions have been developed. The Givoli-Neta formulation [64] and the Hagstrom-Warburton absorbing condition [65, 66], both derived from the Higdon condition, use auxiliary variables and functions to eliminate the computation of high order derivatives from high order local boundary conditions.

In the current instance Partition of Unity Infinite elements will be used. The use of conventional Infinite Elements is well established as a termination for traditional Finite Element models with and without mean flow [30, 35]. They are used to mesh an infinite domain with a finite number of elements but are generally unable to model the solution accurately in the near field where the sound source is located. In practice, the unbounded

domain is therefore subdivided into an inner region and an outer region. A Partition of Unity Finite Element method will be developed in this thesis for the inner region and a Mapped Partition of Unity Infinite Element method for the outer region. The latter is based on the Mapped Wave Envelope Infinite Element (MWEIE) developed by Astley [30] for the case without mean flow and extended by Eversman [35] to the convected case. Astley et al. [31] subsequently used Legendre polynomials instead of the original Lagrange polynomials, for the radial basis in the infinite element region. This follows improvements in accuracy and conditioning recorded by Shirron and Babuška for related elements [33]. An improved radial basis of this type, formed from shifted Legendre polynomials, is used also in the current formulation, although Dreyer [32, 34] has suggested that the use of Jacobi polynomials leads to even better conditioning of the resulting equations.

2.8 Mapped Infinite Partition of Unity Elements

Unbounded problems Ω will be divided into a finite inner region Ω_i and an infinite outer region Ω_o , separated by an interface Γ [30]. The inner region is partitioned by using Partition of Unity finite elements as described in section 2.5 and the outer region Ω_o is discretized using Partition of Unity Infinite elements that are compatible to the Partition of Unity finite elements on the interface Γ .

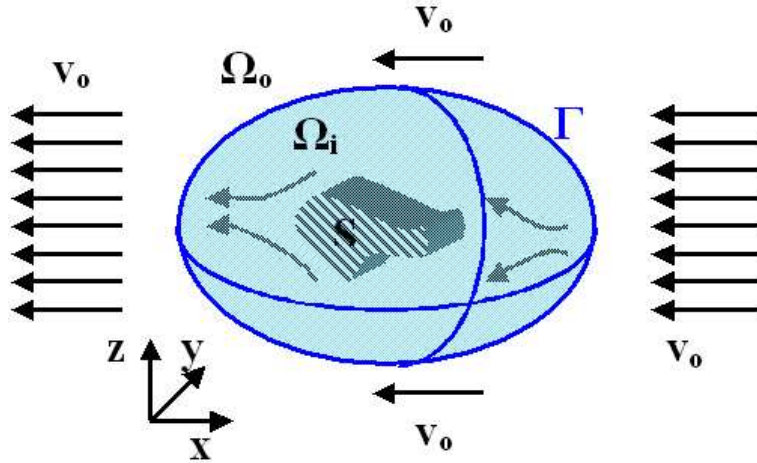


Fig. 2.9. Illustration of a vibrating body of surface S which radiates in an unbounded domain Ω . The infinite region is decomposed into an inner and an outer region (respectively Ω_i and Ω_o). In the outer region, the mean flow is assumed to be uniform while it is allowed to be non-uniform in the inner region.

The inner region contains the geometry of the application and all the sources. The steady mean flow in the outer region is assumed to be uniform and oriented along the x

direction while it is allowed to be non-uniform in the inner region as long as it remains irrotational (figure 2.9).

Following these assumptions, the convected wave formulation becomes, in the outer region:

$$\begin{aligned} & \int_{\Omega_o} \left(\nabla W \cdot \nabla \tilde{\phi}_a - M_0^2 \frac{\partial W}{\partial x} \frac{\partial \tilde{\phi}_a}{\partial x} \right) d\Omega \\ & + \int_{\Omega_o} \left(ikM_0 \left(W \frac{\partial \tilde{\phi}_a}{\partial x} - \frac{\partial W}{\partial x} \tilde{\phi}_a \right) - k^2 W \tilde{\phi}_a \right) d\Omega = 0 \end{aligned} \quad (2.95)$$

There is no boundary integrals as we assume the interface Γ free from boundary conditions and we will choose the shape and weight functions such that the integral over the boundary at infinity vanishes (see section 2.8.4).

The outer region (Ω_o) is partitioned by mapped infinite elements. These infinite elements are mapped such as represented in figure 2.10. Each infinite element is defined in global coordinates by four nodes (1, 2, 3, 4) and four mapping points (5, 6, 7, 8) located on the interface Γ separating the inner and the outer region. Eight other mapping points (1', ..., 8') represent the source locations (focal points for the mapping) and define the infinite radial direction, e.g. orientation (2'2). The numerical integration will be performed on the parent element (ξ, η, ζ) , each infinite element is then mapped on a cubic element (mapping functions are detailed in appendix 10.1).

The approximation of the acoustic potential in the outer region is based on specific shape functions which take into account the decay and the oscillatory behaviour of the radiated waves. A typical infinite element approximation $\tilde{\phi}_h^I$ is created by infinite shape functions Φ_j^I , for all infinite nodes j . The infinite shape function consists of the product of three separate factors:

- a radial function (R) which contains a decay proportional to powers of $\frac{1}{r_o}$ with r_o the distance from the source,
- an outwardly propagating wavelike factor ($e^{-ik\mu}$),
- and a circumferential interpolant (T) defined such that the potential is compatible at the finite element/infinite element interface.

$$\Phi_j^I(\mathbf{x}, \omega, M_0) = R_j(\mathbf{x}) T_j(\mathbf{x}) e^{-ik\mu(\mathbf{x}, M_0)} \quad (2.96)$$

Note that there is more than one unknown coefficient per infinite node, this is detailed in following sections.

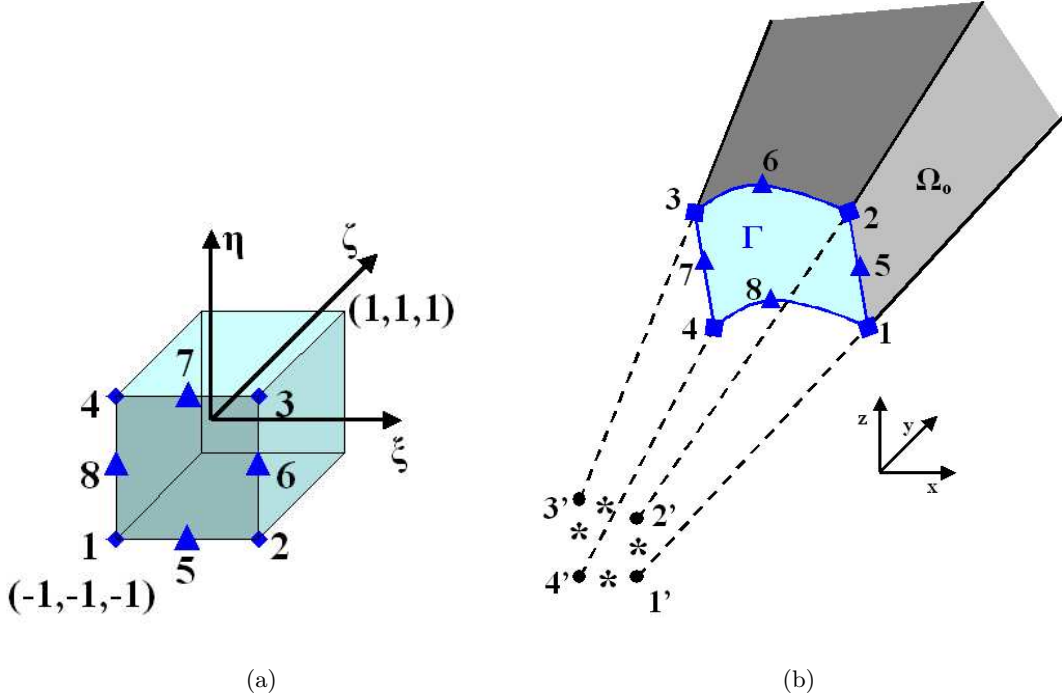


Fig. 2.10. Topology of a three-dimensional infinite element in local (a) and global (b) coordinates.

2.8.1 Radial functions

Following the Wilcox-Atkinson expansion [31], the radial decay should have the form given at equation 2.97 (with a_j constant and r_o the distance from the source point).

$$R_j(\mathbf{x}) \approx \left(\frac{a_1}{r_o}\right) + \left(\frac{a_2}{r_o}\right)^2 + \cdots + \left(\frac{a_{m_0}}{r_o}\right)^{m_0} \quad (2.97)$$

An expansion of this type with m_0 terms contains a radial basis for spherical Bessel functions up to the order $(m_0 - 1)$ [30]. A first order element ($m_0 = 1$) is then able to model accurately the radial behaviour of an acoustic monopole, a second order element to model that of a dipole and so on. Radial approximation 2.97 is constructed at each node j with shifted Legendre polynomials (L_j^d) of order d (figure 2.11). The value of the radial function R_j^d (figure 2.12) on the interface Γ (i.e. $\zeta = -1$) is equal to zero except for $d = 1$. In this case, L_j^1 is set to 1.

$$R_j^d(\mathbf{x}) = \frac{1 - \zeta}{2} L_j^d(\zeta) \quad (2.98)$$

$$R_j(\mathbf{x}) = \sum_{d=1}^{m_0} R_j^d(\mathbf{x}) e_{jd} \quad (2.99)$$

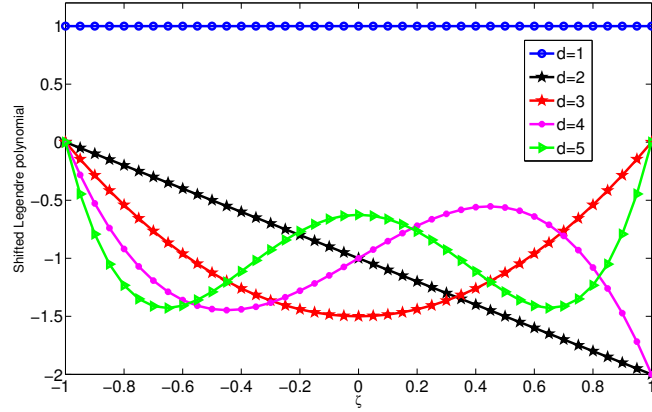


Fig. 2.11. Shifted Legendre polynomials for $d = [1, 5]$ along the radial direction in a parent element: $\zeta = [-1, 1]$

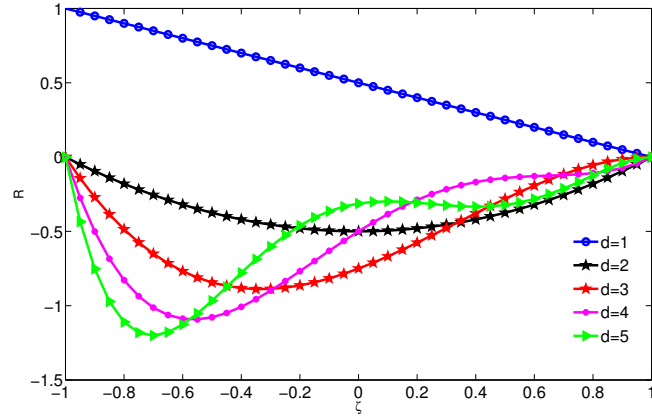


Fig. 2.12. Radial functions for $d = [1, 5]$ along the radial direction in a parent element: $\zeta = [-1, 1]$

2.8.2 Outwardly propagating wavelike factor

The wavelike factor along the infinite edges is chosen to represent outwardly propagating solutions of the convected wave equation. The phase function $\mu(\mathbf{x}, M_0)$ at any position of the infinite element depends the definition of the phase along the infinite edges and mapping functions $S_i(\xi, \eta)$ defined over the base of the infinite element.

$$\mu(\mathbf{x}) = \sum_{i=1}^8 S_i(\xi, \eta) (\Psi_i(\mathbf{x}_i) - \Psi_{1,i}) \quad (2.100)$$

$$\Psi_i(\mathbf{x}_i) = \frac{2\Psi_{1,i}}{1 - \zeta} \quad (2.101)$$

$$\Psi_{1,i} = \frac{1}{1 - M_0^2} [-M_0(x_i - x'_i) + H_{1,i}] \quad (2.102)$$

$$H_{1,i} = \sqrt{(x_i - x'_i)^2 + (1 - M_0^2) ((y_i - y'_i)^2 + (z_i - z'_i)^2)} \quad (2.103)$$

with (x'_i, y'_i, z'_i) the coordinates of source points and (x_i, y_i, z_i) the coordinates of the four nodes and the four mapping points lying on the interface Γ (fig. 2.10). The development of this results is shown in appendix 10.3.

2.8.3 Circumferential functions

The circumferential functions must ensure the continuity of the acoustic potential through the interface Γ . Note that, by definition on this interface, the wavelike factor equals to 1 (because $\mu = 0$) and the radial functions equal to zero except for $d = 1$.

The originality of the Mapped Infinite Partition of Unity Method consists in the way that the circumferential shape functions are defined. When $d = 1$, the circumferential functions of a node j consist of the product of nodal Partition of Unity functions and enrichment functions. The enrichment is chosen to be the same as the enrichment defined at the same node j but inside the inner region (figure 2.13).

$$T_j^1 = N_j(\mathbf{x}_\Gamma) \sum_{b=1}^{n(j)} a_b V_{jb}(\mathbf{x}_\Gamma) \quad (2.104)$$

where \mathbf{x}_Γ is the projection of the coordinate \mathbf{x} on the interface Γ .

Note that this infinite circumferential function is constant along the radial direction. This means that the Partition of Unity and enrichment functions are constructed over the base of the infinite element and taken constant within the radial direction. This ensures the compatibility between the circumferential function and the projection on the interface Γ of the inner shape functions. Both “inner” and “outer” functions take the same values along the interface Γ . The degrees of freedom of the infinite shape functions with $d = 1$ are chosen to be the same as those of the inner nodes lying on the interface. This prescribes the continuity.

Radial functions for which $d > 1$ are equal to zero on the interface Γ . The continuity does not depend on the circumferential functions linked to radial functions with $d > 1$. Circumferential functions for $d > 1$ are defined by:

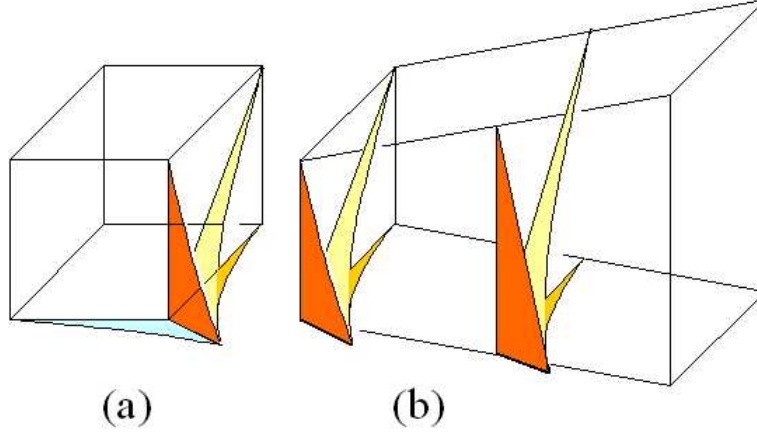


Fig. 2.13. This figure illustrates the continuity between the inner and the outer regions. On the left side (a), the figure represents an inner element with an enrichment function at the node j : $(V_{jb}(\mathbf{x}))$. Figure (b) shows the outer infinite element which shares the nodes lying on the interface Γ of element (a). The function which is presented is the circumferential function $V_{jb}(\mathbf{x}_\Gamma)$. This function is equal to the values taken by the inner enrichment V_{jb} on the interface and is constant along the radial direction.

$$T_j^2 = N_j(\mathbf{x}_\Gamma) \sum_{b=1}^{b_0} a_b N_j^{(b-1)}(\mathbf{x}_\Gamma) \quad (2.105)$$

where b_0 is a parameter defining the circumferential order of the infinite functions. Note that $N_j^{(b)}$ corresponds to the b^{th} power of the Partition of Unity function at node j .

2.8.4 Infinite shape and weighting functions

Equation 2.96 describes the fact that an infinite shape function is composed of the product of radial functions, circumferential functions and a wave factor. We decide to define two different circumferential functions depending on the radial degree d varying between 1 and the radial order m_0 . In the case where $d = 1$ (first radial order), the circumferential shape function is taken to be the projection of the Partition of Unity shape functions on the base of the element as it is represented in figure 2.13. The other circumferential shape functions ($d > 1$) are described by equation 2.105.

The infinite shape function at node j can then be written as:

$$\Phi_j^I(\mathbf{x}, \omega, M_0) = \left(R_j^{d=1}(\mathbf{x}) T_j^1(\mathbf{x}) + \sum_{d=2}^{m_0} R_j^d(\mathbf{x}) T_j^2(\mathbf{x}) \right) e^{-ik\mu(\mathbf{x}, M_0)} \quad (2.106)$$

The Mapped Infinite Partition of Unity approximation is given by:

$$\begin{aligned} \tilde{\phi}_h^I(\mathbf{x}, \omega, M_0) = & \sum_{j=1}^{nni} e^{-ik\mu(\mathbf{x}, M_0)} \left(R_j^1(\mathbf{x}) N_j(\mathbf{x}_\Gamma) \sum_{b=1}^{n(j)} V_{jb}(\mathbf{x}_\Gamma) e_{j1b} \right. \\ & \left. + \sum_{d=2}^{m_0} R_j^d(\mathbf{x}) \sum_{b=1}^{b_0} (N_j^b(\mathbf{x}_\Gamma)) e_{jdb} \right) \end{aligned} \quad (2.107)$$

where nni is the number of infinite nodes. The coefficients e_{jdb} are the unknowns of the outer region. In fact, at an infinite node j , there is m_0 radial shape functions. For the first radial shape function ($d = 1$), there are $n(j)$ circumferential shape functions and then $n(j)$ unknowns e_{j1b} with $b = 1 : n(j)$. Note that the b unknowns of infinite node j (e_{j1b}) correspond to existing degrees of freedom, those from the inner node sharing the same location than the infinite node j . For each other infinite radial function ($d = 2 : m_0$) at node j there is b_0 circumferential shape functions. The unknown coefficient of the infinite shape function of node j corresponding to the b^{th} circumferential function of the d^{th} radial order is e_{jdb} .

It is convenient to rewrite equation (2.107) as

$$\tilde{\phi}_h^I(\mathbf{x}, \omega, M_0) = \sum_{j=1}^{nni} \left(\sum_{b=1}^{n(j)} \Upsilon_{j1b}(\mathbf{x}) e_{j1b} + \sum_{d=2}^{m_0} \sum_{b=1}^{b_0} \Upsilon_{jdb}(\mathbf{x}) e_{jdb} \right) \quad (2.108)$$

where

$$\begin{cases} \Upsilon_{jdb}(\mathbf{x}) = e^{-ik\mu(\mathbf{x}, M_0)} R_j^d(\mathbf{x}) N_j(\mathbf{x}_\Gamma) V_{jb}(\mathbf{x}_\Gamma) & \text{for } d = 1 \\ \Upsilon_{jdb}(\mathbf{x}) = e^{-ik\mu(\mathbf{x}, M_0)} R_j^d(\mathbf{x}) N_j^b(\mathbf{x}_\Gamma) & \text{for } d > 1 \end{cases} \quad (2.109)$$

The definition of the approximation in the infinite elements can be further simplified by noting that the summation over the indices could be combined to give a summation over a single index α^I say which varied from 1 to n_d^I where n_d^I is the total number of degree of freedom of the model in the outer region (the sum of the number of unknowns at each infinite node). The way in which the index is assigned to the single index α^I is unimportant provided that there is a one to one mapping. The approximation in the infinite outer region then becomes ($\Phi_{\alpha^I}^I$ and e_{α^I} denote Υ_{jdb} and e_{jdb})

$$\tilde{\phi}_h^I(\mathbf{x}, \omega, M_0) = \sum_{\alpha^I=1}^{n_d^I} \Phi_{\alpha^I}^I e_{\alpha^I} \quad (2.110)$$

The infinite weighting functions ($W_{\alpha^I}^I$) are chosen to be the complex conjugates of the infinite shape functions ($\Phi_{\alpha^I}^I$), following a conjugated Galerkin scheme. This choice leads to the cancellation of wavelike terms ($e^{\pm ik\mu}$) in the infinite integrals.

$$W_{\alpha^I}^I(\mathbf{x}, \omega) = G(\mathbf{x}) (\Phi_{\alpha^I}^I(\mathbf{x}, \omega, M_0))^* \quad (2.111)$$

where G is a geometric factor chosen to conduct to proper integrals for the infinite elements.

$$G(\mathbf{x}) = \left(\frac{H_{1,i}}{\sqrt{(x-x_0)^2 + (1-M_0^2)((y-y_0)^2 + (z-z_0)^2)}} \right)^q \quad q \geq 3 \quad (2.112)$$

The combination of the Wilcox-Atkinson expansion 2.97 and the solution of the convected wave element in the outer region 10.21 leads to the following asymptotic dependencies of the shape functions:

$$\begin{aligned} \phi_{\alpha I}^I(\mathbf{x}, \omega) &\approx f \frac{e^{-ik\mu}}{R'} \\ W_{\alpha I}^I(\mathbf{x}, \omega) &\approx G f \frac{e^{ik\mu}}{R'} \end{aligned} \quad (2.113)$$

where f represents the variation of the shape functions in the circumferential direction and $R' = \sqrt{\frac{x^2}{\beta^2} + y^2 + z^2}$.

The factor G is taken to be proportional to $\frac{1}{R'^q}$. The parameter q is chosen such that the integral over the boundary vanishes at infinity and to lead to proper integrals in the outer region (eq. 2.95) [30, 35].

2.9 Axisymmetric formulation

The convected wave equation (2.32) is solved for axisymmetric geometries. The three-dimensional solution therefore can be computed on the two-dimensional domain Ω . The whole three-dimensional domain is obtained by rotating the computational domain Ω and boundary S (figure 2.14) around the axial z axis (z and r are axial and radial coordinates.).

We assume that the steady mean flow variables do not vary in the azimuthal direction. The acoustic variables however are assumed to vary as $e^{-im\theta}$, m being the azimuthal order. The three-dimensional acoustic perturbation is also assumed to vary harmonically in time with frequency f . The unsteady acoustic velocity potential $\phi_a(\mathbf{x}, t)$ can therefore be written as

$$\phi_a(\mathbf{x}, t) = \Re \left(\tilde{\phi}_a(z, r) e^{i\omega t - im\theta} \right) \quad (2.114)$$

A weighted residual procedure is applied to the three-dimensional convected wave equation 2.32 over the volume of revolution generated by the domain Ω . A complex weighting function $W(z, r)e^{+im\theta}$ is used and the divergence theorem is applied, in the usual way. Since the azimuthal variation of $\tilde{\phi}_a$ and W are as $e^{-im\theta}$ and $e^{+im\theta}$ respectively, all variations with θ are removed from the resulting volume and surface integrals reduce to area and contour

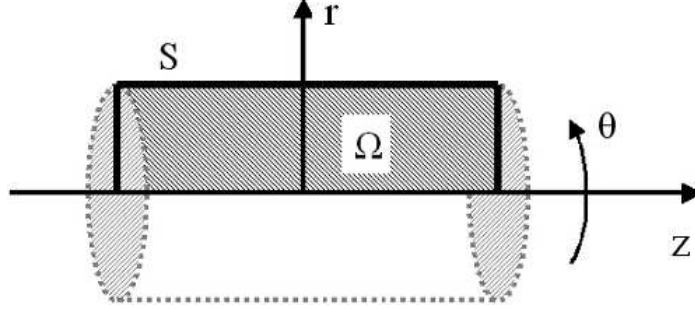


Fig. 2.14. Representation of the geometry of a cylindrical duct obtained by rotating the domain Ω around the axial \mathbf{z} axis

integrals over Ω and S where, S denotes the boundary of Ω in the plane of revolution (excluding the axis of symmetry).

The weighted integral statement is then given by

$$\begin{aligned}
& 2\pi \int_{\Omega} r \left(\left(\rho_0 \nabla \tilde{\phi}_a \right) \cdot \nabla W - \nabla W \cdot \left(\frac{\rho_0}{c_0^2} \mathbf{v}_0 \left(\mathbf{v}_0 \cdot \nabla \tilde{\phi}_a \right) \right) \right) d\Omega \\
& + 2\pi i\omega \int_{\Omega} r \left(\frac{\rho_0}{c_0^2} \left(\mathbf{v}_0 \cdot \nabla \tilde{\phi}_a \right) W - \nabla W \cdot \left(\frac{\rho_0}{c_0^2} \mathbf{v}_0 \tilde{\phi}_a \right) \right) d\Omega \\
& - 2\pi\omega^2 \int_{\Omega} r \left(\frac{\rho_0}{c_0^2} \tilde{\phi}_a W \right) d\Omega \\
& = 2\pi \int_S r W \rho_0 \left(-\frac{1}{c_0^2} \mathbf{v}_0 \cdot \mathbf{n} \left(\mathbf{v}_0 \cdot \nabla \tilde{\phi}_a \right) + \nabla \tilde{\phi}_a \cdot \mathbf{n} \right) dS \\
& - 2\pi i\omega \int_S r \left(W \frac{\rho_0}{c_0^2} \mathbf{v}_0 \tilde{\phi}_a \cdot \mathbf{n} \right) dS \quad \forall W \in \mathcal{V}
\end{aligned} \tag{2.115}$$

where \mathcal{V} the Sobolev space H^1 .

Note however that although $\tilde{\phi}_a$ is now a function of z and r only, the operators $\nabla(\cdot)$ and $\nabla \cdot (\cdot)$ in the above equation are the three-dimensional gradient and divergence operators. The prescribed azimuthal variation in the acoustic quantities must therefore be taken into account when interpreting quantities such as $\nabla \tilde{\phi}_a$ in the above equation. That is to say, the operator ∇ when is applied to $\tilde{\phi}_a$ includes a third component in the θ direction. This operator will be called ∇_{θ} and must be written

$$\nabla_{\theta} \tilde{\phi}_a = \frac{\partial \tilde{\phi}_a}{\partial z} \mathbf{1}_z + \frac{\partial \tilde{\phi}_a}{\partial r} \mathbf{1}_r - \frac{im}{r} \tilde{\phi}_a \mathbf{1}_{\theta}, \tag{2.116}$$

where $\mathbf{1}_z$, $\mathbf{1}_r$ and $\mathbf{1}_{\theta}$ are unit vectors in the axial, radial and azimuthal directions, respectively. The acoustic pressure amplitude \tilde{p}_a can be recovered, if required, from the acoustic potential $\tilde{\phi}_a$ through the linearised momentum equation 2.26

$$\tilde{p}_a = -\rho_0 \left(i\omega \tilde{\phi}_a + \mathbf{v}_0 \cdot \nabla_\theta \tilde{\phi}_a \right) \quad (2.117)$$

Since the weighting function W has a prescribed azimuthal variation of $e^{+im\theta}$, care must be taken when interpreting ∇W which must in fact be written

$$\nabla_\theta W = \frac{\partial W}{\partial z} \mathbf{1}_z + \frac{\partial W}{\partial r} \mathbf{1}_r + \frac{im}{r} W \mathbf{1}_\theta. \quad (2.118)$$

2.9.1 The Partition of Unity Method

The Partition of Unity Method has been presented in section 2.5 for the three-dimensional case. The same developments can be done in the axisymmetric case. Here are the major points needed to consider.

The Partition of Unity approximation is built as the product of Partition of Unity functions $N_j(z, r)$ and enrichment functions $V_{jl}(z, r)$:

$$\tilde{\phi}^h = \sum_{j=1}^{nodes} N_j(\mathbf{z}) \sum_{l=1}^{n(j)} V_{jl}(\mathbf{z}) e_{jl} \quad (2.119)$$

where $nodes$ is the number of nodes, $n(j)$ denotes the number of enrichment functions V_{jl} composing the local approximation space of node j .

The Partition of Unity approximation is based on the property that the nodal shape functions $N_j(\mathbf{z})$ (where $\mathbf{z} = (z, r)$) of a Finite Element mesh satisfy

$$\sum_{j=1}^{nodes} N_j(\mathbf{z}) = 1. \quad (2.120)$$

A set of enrichment functions is attributed to each node of the mesh. This can differ from one node to another. For instance, the following second order enrichment (2.121), with (z_j, r_j) are the coordinates of the node j , means that six degrees of freedom are attributed to the node j .

$$V_j(\mathbf{z}) = \{1, (z - z_j), (r - r_j), (z - z_j)^2, (r - r_j)^2, (z - z_j)(r - r_j)\} \quad (2.121)$$

The method is implemented with quadrilateral elements and the degrees of freedom are attributed to four nodes located at the vertices of the element. Four additional points can be added to generate a mapped element (figure 2.15). These additional geometrical points do not contain any degrees of freedom but give an information about the geometry

of the element. The geometry of the element is then based on quadratic mapping functions (see appendix 10.1), with respect to the four nodes and the four mapping points. The aim of using such elements is to better represent the geometry of the boundary, and hence to improve the accuracy of the numerical solution [26]. If mapping functions of mapped elements are quadratic, the Partition of Unity N_j functions remains bilinear.

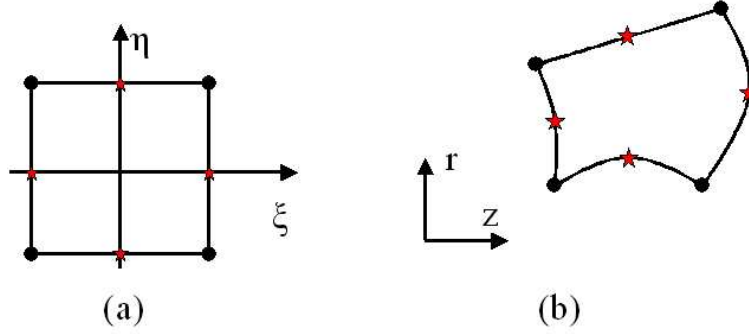


Fig. 2.15. Topology of a mapped finite element (b) and its parent element (a)

Before proceeding further, it is convenient to rewrite expression (2.119) as

$$\tilde{\phi}^h = \sum_{j=1}^{nodes} \sum_{l=1}^{n(j)} \Phi_{jl}(\mathbf{z}) e_{jl} \quad \text{where} \quad \Phi_{jl}(\mathbf{z}) = N_j(\mathbf{z}) V_{jl}(\mathbf{z}). \quad (2.122)$$

This can be further simplified by noting that the double summation over the indices j and l could be combined to give a summation over a single index α say which varied from 1 to n_u where n_u is the total number of degree of freedom of the model (the sum of the number of enrichment functions at each node). The way in which the index pair (j, l) is assigned to the single index α is unimportant provided that there is a one to one mapping. Expression (2.122) then becomes

$$\tilde{\phi}^h = \sum_{\alpha=1}^{n_u} \Phi_{\alpha}(\mathbf{x}) e_{\alpha} \quad (2.123)$$

where ϕ_{α} and e_{α} denote ϕ_{jl} and e_{jl} . Trial solution (2.123) is then substituted into variational formulation (2.115) and the resulting expression evaluated for a complete set of weighting functions ($W_{\beta}(\mathbf{z}), \beta = 1, 2..n_u$). This leads to a set of linear equations

$$([\mathbf{K}] + i\omega [\mathbf{C}] - \omega^2 [\mathbf{M}]) \{\phi_a\} = \{\mathbf{F}\} \quad (2.124)$$

where $\{\phi_a\}$ is a vector of length n_u which contains the unknown degrees of freedom e_{α} .

The matrices $[\mathbf{K}]$, $[\mathbf{C}]$, $[\mathbf{M}]$ and $\{\mathbf{F}\}$ have components

$$K_{\alpha\beta} = 2\pi \int_{\Omega} r \rho_0 \nabla_{\theta} W_{\alpha} \cdot \nabla_{\theta} \Phi_{\beta} d\Omega - 2\pi \int_{\Omega} r \rho_0 \left(\frac{\mathbf{v}_0}{c_0} \cdot \nabla_{\theta} W_{\alpha} \right) \left(\frac{\mathbf{v}_0}{c_0} \cdot \nabla_{\theta} \Phi_{\beta} \right) d\Omega \quad (2.125)$$

$$C_{\alpha\beta} = 2\pi \int_{\Omega} \frac{r \rho_0}{c_0^2} (W_{\alpha} (\nabla_{\theta} \Phi_{\beta} \cdot \mathbf{v}_0) - \Phi_{\alpha} (\nabla_{\theta} W_{\beta} \cdot \mathbf{v}_0)) d\Omega \quad (2.126)$$

$$M_{\alpha\beta} = 2\pi \int_{\Omega} \frac{r \rho_0}{c_0^2} W_{\alpha} \Phi_{\beta} d\Omega \quad (2.127)$$

$$F_{\alpha} = 2\pi \int_S r W_{\alpha} \left[\left(\rho_0 \nabla_{\theta} \tilde{\phi}_a \right) - \frac{\rho_0}{c_0^2} \mathbf{v}_0 \left(\mathbf{v}_0 \cdot \nabla_{\theta} \tilde{\phi}_a \right) \right] \cdot \mathbf{n} dS - 2\pi i \omega \int_S \frac{r \rho_0}{c_0^2} W_{\alpha} \left[\tilde{\phi}_a \right] (\mathbf{v}_0 \cdot \mathbf{n}) dS. \quad (2.128)$$

where the terms in square brackets $[\]$ in the expression for F_{α} will be further modified by the application of boundary conditions.

The current formulation is completed by defining the weighting functions to be the same as the trial basis functions, i.e. a traditional Petrov-Galerkin scheme in which

$$W_{\alpha}(\mathbf{z}) = \Phi_{\alpha}(\mathbf{z}), \alpha = 1, 2..n_u. \quad (2.129)$$

This reduces to a conventional linear Finite Element formulation for the ‘degenerated’ case when a constant is used as the unique enrichment function at each node, i.e. when $V_j(\mathbf{z}) = \{1\}$.

2.9.2 Application of the boundary conditions

Boundary conditions to consider correspond to prescribed surface accelerations and prescribed modal descriptions of the sound field at intake and outlet planes. The current method can also deal readily with more complex boundary conditions such as the presence of a locally reacting surface in the presence of grazing flow (the ‘Myers’ condition [39, 40]).

Surface acceleration

We consider the case where an impervious surface located at (S_v) vibrates with a prescribed, time harmonic normal acceleration of amplitude \tilde{a}_n . The corresponding normal

displacement, $u_n = \tilde{u}_n e^{i\omega t}$, is given by $\tilde{u}_n = -\frac{\tilde{a}_n}{\omega^2}$. Myers and Eversman in their development of local impedance boundary conditions for flow problems [39, 41] showed that the normal velocity of the vibrating surface and the normal particle velocity in the fluid at the inner edge of an infinitely thin boundary layer are consistent provided that the normal acoustic velocity on the surface $\tilde{v}_{a,n}$ and the normal particle displacement are related by

$$\tilde{v}_{a,n} = \nabla_\theta \tilde{\phi}_a \cdot \mathbf{n} = i\omega \tilde{u}_n + \mathbf{v}_0 \cdot \nabla_\theta \tilde{u}_n - \tilde{u}_n \mathbf{n} \cdot (\mathbf{n} \cdot \nabla_\theta) \mathbf{v}_0. \quad (2.130)$$

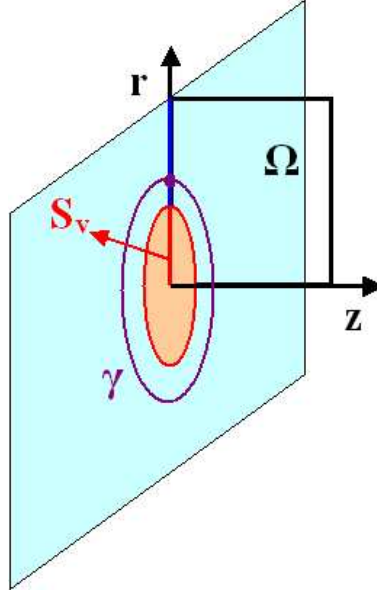


Fig. 2.16. Representation vibrating piston mounted on a hard wall. The vibrating piston is in pink surrounded by a purple contour γ . This figure shows the three-dimensional geometry of the application and the axisymmetric computational domain Ω needed for the numerical simulation

If the vibrating wall is stationary (in a mean sense) and impervious then ($\mathbf{v}_0 \cdot \mathbf{n} = 0$), and in these circumstances the contribution to F_α defined by expression (2.128) becomes [41]:

$$F_\alpha = -2\pi \int_{S_v} r \rho_0 \frac{\tilde{a}_n}{\omega^2} (i\omega W_\alpha - \mathbf{v}_0 \cdot \nabla_\theta W_\alpha) dS + \int_\gamma \left(\mathbf{n} \times W_\alpha \rho_0 \frac{\tilde{a}_n}{\omega^2} \mathbf{v}_0 \right) \cdot d\boldsymbol{\gamma} \quad (2.131)$$

where γ is a 3-D boundary curve which encloses the surface of revolution generated by the vibrating boundary S . Figure 2.16 illustrates a vibrating piston: the three-dimensional geometry - the axisymmetric computational domain - the contour γ - the boundary S_v . The second integral vanishes if the bounding curve γ can be constructed so that it lies on a hard wall, as it is always the case if the vibrating segment is of finite length [41]. Note also that in the case of a rigid surface ($\tilde{a}_n = 0$) both integrals vanish and there is

no contribution to F_α . This confirms that an acoustically ‘hard’ boundary is the ‘natural’ condition for this formulation.

Vibrating walls can also be prescribed by the knowledge of the harmonic normal displacement \tilde{u}_n or velocity \tilde{w}_n of the wall. This is done easily by taking into account the following relations:

$$\begin{aligned} a_n &= \frac{\partial^2 (\tilde{u}_n e^{i\omega t})}{\partial t^2} = -\omega^2 u_n \\ a_n &= \frac{\partial (\tilde{w}_n e^{i\omega t})}{\partial t} = i\omega w_n \end{aligned} \quad (2.132)$$

Admittance boundary conditions

Acoustic absorbants are modelled by admittance coefficients A_n . At the soft wall, the pressure is related to the wall velocity through the normal admittance:

$$\begin{aligned} \tilde{w}_n &= A_n \tilde{p}_a \quad \text{or} \\ \tilde{u}_n &= -\frac{A_n}{i\omega} \rho_0 \left(i\omega \tilde{\phi}_a + \mathbf{v}_0 \cdot \nabla_\theta \tilde{\phi}_a \right) \end{aligned} \quad (2.133)$$

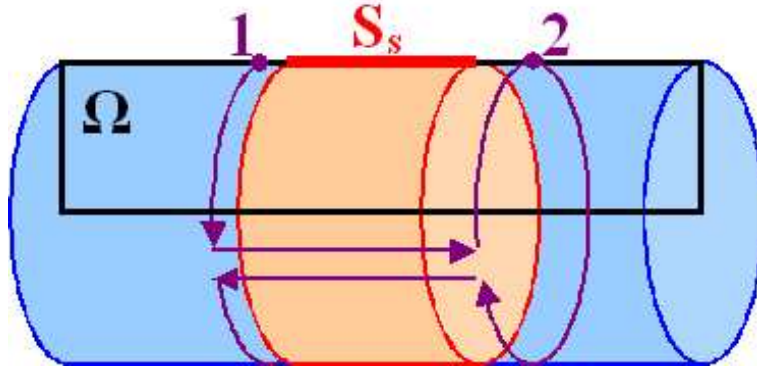


Fig. 2.17. Representation of a duct partially lined. The soft wall is in pink surrounded by a purple contour. In axisymmetric applications, only the line (S_s) and points (1, 2) have to be considered.

The wall displacement \tilde{u}_n is related to particle acoustic velocity $\mathbf{v}_a \cdot \mathbf{n}$ through the relation 2.130, with $\nabla_\theta \tilde{\phi}_a \cdot \mathbf{n} = \mathbf{v}_a \cdot \mathbf{n}$. As it has been done for the wall motion boundary condition, the admittance boundary is impermeable to the flow. We assume that the steady mean flow is tangent to the boundary.

$$\begin{aligned}
-2\pi \int_{S_s} r \rho_0 W_\alpha \tilde{\mathbf{v}}_a \cdot \mathbf{n} d\Gamma &= 2\pi \int_{S_s} r A_n \rho_0^2 \left(W_\alpha \mathbf{v}_0 \cdot \nabla_\theta \tilde{\phi}_a - \tilde{\phi}_a \mathbf{v}_0 \cdot \nabla_\theta W_\alpha \right) dS \\
&+ 2\pi i \omega \int_{S_s} r A_n \rho_0^2 \tilde{\phi}_a W_\alpha dS \\
&- \frac{2\pi}{i\omega} \int_{S_s} r A_n \rho_0^2 \left(\mathbf{v}_0 \cdot \nabla_\theta \tilde{\phi}_a \right) \left(\mathbf{v}_0 \cdot \nabla_\theta W_\alpha \right) dS \\
&- 2\pi \left[r \frac{A_n \rho_0^2 W_\alpha \mathbf{v}_{0,t}}{i\omega} \left(i\omega \tilde{\phi}_a + \mathbf{v}_0 \cdot \nabla_\theta \tilde{\phi}_a \right) \right] \Big|_1 \\
&+ 2\pi \left[r \frac{A_n \rho_0^2 W_\alpha \mathbf{v}_{0,t}}{i\omega} \left(i\omega \tilde{\phi}_a + \mathbf{v}_0 \cdot \nabla_\theta \tilde{\phi}_a \right) \right] \Big|_2 \quad (2.134)
\end{aligned}$$

with $v_{0,t}$, the tangential part of the mean flow along the wall.

The previous remarks 2.3.1 concerning the line integration stands also here. If it exists a surrounding contour which lies on a hard wall, then the terms in brackets $[\]$ vanish. This is illustrated in figure 2.17. A soft wall of finite length is inserted in a cylindrical duct. The figure illustrates the three-dimensional geometry, the axisymmetric computational domain, the soft wall boundary S_s and contour γ . $\tilde{\phi}_a$ in expression 2.134 is the amplitude of the acoustic potential which is unknown on S_s . It is replaced by the approximation $\tilde{\phi}_h$ (eq. 2.123).

Modal boundary conditions

We consider a case where the flow in the duct is uniform and oriented with the duct axis z . S_M is the cross-section, perpendicular to the z axis. The expression for F_α defined by expression (2.128) then reduces to

$$F_\alpha = -2\pi \int_{S_M} r \rho_0 W_\alpha \left(ik M_0 \tilde{\phi}_a - \beta^2 \frac{\partial \tilde{\phi}_a}{\partial z} \right) dS \quad (2.135)$$

where M_0 is the Mach number of the uniform mean flow in the duct.

If S_M supports a modal boundary condition, the acoustic potential can be described by a combination of modes:

$$\tilde{\phi}_a \Big|_{S_M} = \sum_{n=1}^{\infty} \left(A_n^+ E_n^+(r) e^{-ik_z^+ n z} + A_n^- E_n^-(r) e^{-ik_z^- n z} \right) \quad (2.136)$$

The summation over the circumferential index m has been removed since axisymmetric computations can only deal with one value of the angular mode number at each computation.

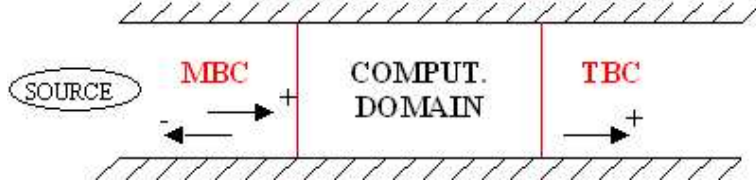


Fig. 2.18. Infinite duct modelling (MBC: Modal Boundary Condition; TBC: Transmitted Boundary Condition)

$$\left. \frac{\partial \tilde{\phi}_a}{\partial z} \right|_{S_M} = \sum_{n=1}^{\infty} \left(-ik_{z,n}^+ A_n^+ E_n^+(r) e^{-ik_{z,n}^+ z} - ik_{z,n}^- A_n^- E_n^-(r) e^{-ik_{z,n}^- z} \right) \quad (2.137)$$

where A_n^+ , A_n^- are respectively the known (prescribed) and unknown (reflected) amplitudes of the downstream and upstream modes, $E_n^+ e^{-ik_{z,n}^+ z}$ and $E_n^- e^{-ik_{z,n}^- z}$, respectively. As associated modes are evanescent above the cut-off frequency, the infinite summation can be truncated.

Such a boundary condition adds unknowns (corresponding to the reflected amplitudes) to the system. A new set of equations has then to be added. We use a weighted integral form of equation (2.136), using as weighting functions $\hat{E}_q = i\rho_0 (kM_0 + \beta^2 k_{z,q}^-) E_q^-$. The system to solve becomes:

$$\begin{bmatrix} [\mathbf{D}_M] & [\mathbf{C}_M] \\ [\mathbf{A}_M] & ([\mathbf{K}] + i\omega [\mathbf{C}] - \omega^2 [\mathbf{M}]) \end{bmatrix} \begin{Bmatrix} \{\mathbf{a}_M\} \\ \{\phi_a\} \end{Bmatrix} = \begin{Bmatrix} \{\mathbf{E}_M\} \\ \{\mathbf{B}_M\} \end{Bmatrix} + \begin{Bmatrix} \{\mathbf{0}\} \\ \{\mathbf{F}\} \end{Bmatrix} \quad (2.138)$$

where $\{\mathbf{F}\}$ corresponds to the contribution of all solicitations excepted the modal boundary condition.

The matrices coming from the modal boundary conditions are:

$$A_{M,\alpha\gamma} = 2\pi i\rho_0 (\beta^2 k_{z,\gamma}^- + M_0 k) \int_{S_M} r W_\alpha E_\gamma^- dS \quad (2.139)$$

$$B_{M,\alpha} = -2\pi i\rho_0 \sum_{a=1}^{N_M} A_a^+ (\beta^2 k_{z,a}^+ + M_0 k) \int_{S_M} r W_\alpha E_a^+ dS \quad (2.140)$$

$$C_{M,\alpha\gamma} = 2\pi i\rho_0 (\beta^2 k_{z,\alpha}^- + M_0 k) \int_{S_M} r \Phi_\gamma E_\alpha^- dS \quad (2.141)$$

$$D_{M,\alpha\gamma} = -2\pi i\rho_0 (\beta^2 k_{z,\alpha}^- + M_0 k) \int_{S_M} r E_\alpha^- E_\gamma^- dS \quad (2.142)$$

$$E_{M,\alpha} = 2\pi i\rho_0 (\beta^2 k_{z,\alpha}^- + M_0 k) \sum_{a=1}^{N_M} A_a^+ \int_{S_M} r E_a^+ E_\alpha^- dS \quad (2.143)$$

where \mathbf{W} and Φ are the Partition of Unity shape functions (equation 2.123). \mathbf{D} is diagonal for cylindrical cross sections as radial modes are Bessel functions which are orthogonal. Matrices \mathbf{A}_M , \mathbf{C}_M , \mathbf{D}_M are respectively of size $(n_u \times N_M)$, $(N_M \times n_u)$ and $(N_M \times N_M)$, while vectors \mathbf{B}_M and \mathbf{E}_M have the following sizes : $(n_u \times 1)$ and $(N_M \times 1)$.

Radial modes E_n^\pm are solutions of the three-dimensional convected wave equation. Axisymmetric radial modes are then equal to the three-dimensional ones (see section 2.6.1).

A similar development is done for the transmitted boundary condition except that, in this case, the amplitudes A_n^- are set to zero since it is assumed that there are no waves coming from the TBC region. Illustration of the concept of modal and transmitted boundary conditions is shown in figure 2.18.

2.9.3 Mapped Infinite Partition of Unity Elements

Unbounded problems Ω will be divided into a finite inner region Ω_i and an infinite outer region Ω_o (figure 2.19), separated by an interface Γ [30]. The inner region is partitioned by using Partition of Unity finite elements as described in section 2.9.1 and the outer region Ω_o is modelled using Partition of Unity infinite elements that are compatible to the Partition of Unity finite elements on the interface Γ .

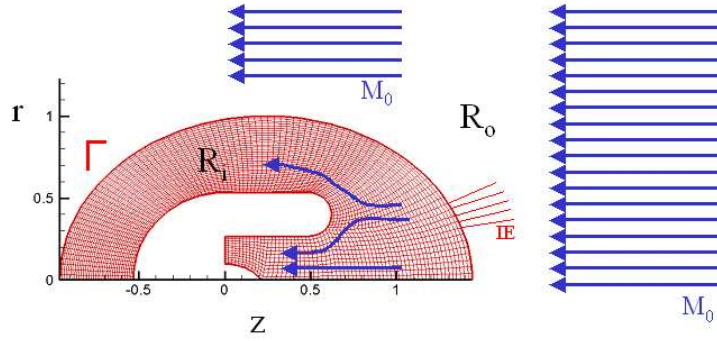


Fig. 2.19. Computational domain of an axisymmetric turbofan radiating in an infinite moving medium.

The inner region contains the geometry of the application and all the acoustic sources. The flow in the outer region is assumed to be uniform and oriented along the axial z direction.

Following these assumptions, the outer region formulation becomes [35]:

$$\begin{aligned}
 & 2\pi \int_{\Omega_o} r \left(\nabla_\theta W \cdot \nabla_\theta \tilde{\phi}_h - M_0^2 \frac{\partial W}{\partial z} \frac{\partial \tilde{\phi}_h}{\partial z} \right) d\Omega \\
 & + 2\pi \int_{\Omega_o} r \left(ikM_0 \left(W \frac{\partial \tilde{\phi}_h}{\partial z} - \frac{\partial W}{\partial z} \tilde{\phi}_h \right) - k^2 W \tilde{\phi}_h \right) d\Omega = 0 \quad (2.144)
 \end{aligned}$$

The infinite element is mapped such as represented in figure 2.20. The outer region (Ω_o) is partitioned by mapped infinite elements (fig. 2.20(a)). Each infinite element is defined in

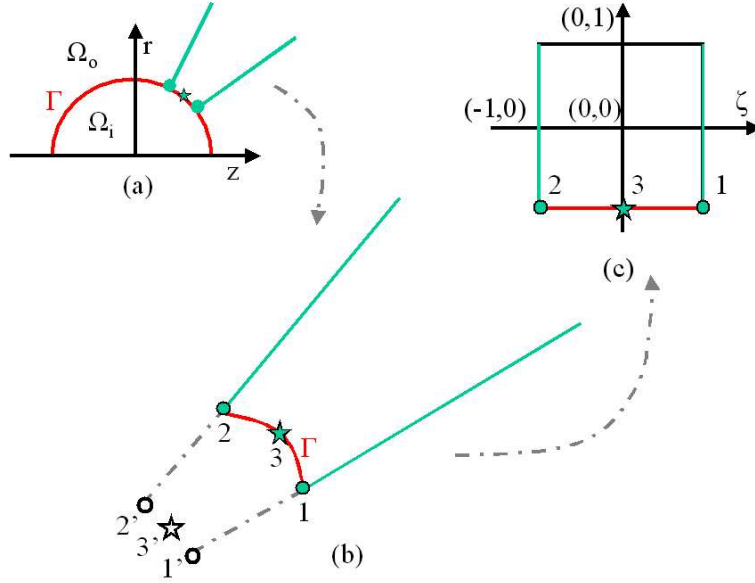


Fig. 2.20. Topology of an infinite element and its parent element: global coordinates of nodes (1 or 2) or mapping point (3) are (z_i, r_i) and source points ($1', 2'$ or $3'$) are (z'_i, r'_i)

global coordinates (fig. 2.20(b)) by two nodes (1, 2) and one mapping point (3). They are located on the interface separating the inner and the outer region. Three other mapping points ($1', 2', 3'$) represent the source location (focal point for the mapping) and the infinite radial direction, e.g. orientation ($2'2$). The numerical integration is performed on the parent element (ξ, η) , each infinite element is then mapped on a square element (fig. 2.20(c)).

The approximation of the acoustic potential in the outer region is based on specific shape functions which take into account the decay and the oscillatory behaviour of the radiated waves. A Typical infinite element approximation $\tilde{\phi}_h^I$ is created by infinite shape functions Φ_j^I , for all infinite nodes j . This infinite shape function consists of the product of three separate factors:

- a radial function (R) which contains a decay proportional to powers of $\frac{1}{r_o}$ with r_o the distance from the source,
- an outwardly propagating wavelike factor ($e^{-ik\mu}$),
- and a circumferential interpolant (T) defined such that the potential is compatible at the finite element/infinite element interface.

$$\Phi_j^I(\mathbf{z}, \omega, M_0) = R_j(\mathbf{z}) T_j(\mathbf{z}) e^{-ik\mu(\mathbf{z}, M_0)} \quad (2.145)$$

Radial functions

Following the same developments as those made for the three-dimensional case (section 2.8.1), the radial functions are given by:

$$R_j^d(\mathbf{z}) = \frac{1-\eta}{2} L_j^d(\eta) \quad (2.146)$$

$$R_j(\mathbf{z}) = \sum_{d=1}^{m_0} R_j^d(\mathbf{z}) e_{jd} \quad (2.147)$$

Outwardly propagating wavelike factor

The definition of the phase function $\mu(\mathbf{z}, M_0)$ at any position of the infinite element depends on mapping functions $S_i(\xi)$ defined over the two nodes and the mapping point creating the base of the element and solutions of the convected wave equation along the radial direction (η).

$$\mu(\mathbf{z}, M_0) = \sum_{i=1}^3 S_i(\xi) (\Psi_i(\mathbf{z}_i) - \Psi_{1,i}) \quad (2.148)$$

$$\Psi_i(\mathbf{z}_i) = \frac{2\Psi_{1,i}}{1-\eta} \quad (2.149)$$

$$\Psi_{1,i} = \frac{1}{1-M_0^2} [-M_0(z_i - z'_i) + H_{1,i}] \quad (2.150)$$

$$H_{1,i} = \sqrt{(z_i - z'_i)^2 + \beta^2 (r_i - r'_i)^2} \quad (2.151)$$

with (z'_i, r'_i) the coordinates of source points and (z_i, r_i) the coordinates of the two nodes and the mapping point lying on the interface Γ .

Circumferential functions

The same idea as that presented in section 2.8.3 is used to create axisymmetric circumferential functions. The only difference is that elements are two-dimensional. Circumferential functions for $d > 1$ are then defined by:

$$T_j^2 = N_j(\mathbf{z}_\Gamma) \sum_{b=1}^{b_0} a_b \left(0.5^{b-1} (1 + \xi_0 \xi)^{b-1} \right) \quad (2.152)$$

where b_0 is defined by the user, $\xi_0 = \pm 1$ is the local ξ coordinate of the node j in the infinite parent element and \mathbf{z}_Γ is the projection of the coordinate \mathbf{z} on the interface.

Infinite shape and weighting functions

The Mapped Infinite Partition of Unity approximation is given by:

$$\begin{aligned} \tilde{\phi}_h^I(\mathbf{z}, \omega, M_0) = & \sum_{j=1}^{nni} e^{-ik\mu(\mathbf{z}, M_0)} \left(R_j^1(\mathbf{z}) N_j(\mathbf{z}_\Gamma) \sum_{b=1}^{n(j)} V_{jb}(\mathbf{z}_\Gamma) e_{j1b} \right. \\ & \left. + \sum_{d=2}^{m_0} R_j^d(\mathbf{z}) N_j(\mathbf{z}_\Gamma) \sum_{b=1}^{b_0} \left(0.5^{b-1} (1 + \xi_0 \xi)^{b-1} \right) e_{jdb} \right) \end{aligned} \quad (2.153)$$

where nni is the number of infinite nodes.

It is convenient to rewrite equation (2.107) as

$$\tilde{\phi}_h^I(\mathbf{z}, \omega, M_0) = \sum_{j=1}^{nni} \left(\sum_{b=1}^{n(j)} \Upsilon_{j1b}(\mathbf{z}) e_{j1b} + \sum_{d=2}^{m_0} \sum_{b=1}^{b_0} \Upsilon_{jdb}(\mathbf{z}) e_{jdb} \right) \quad (2.154)$$

where

$$\begin{cases} \Upsilon_{jdb}(\mathbf{z}) = e^{-ik\mu(\mathbf{z})} R_j^d(\mathbf{z}) N_j(\mathbf{z}_\Gamma) V_{jb}(\mathbf{z}_\Gamma) & \text{for } d = 1 \\ \Upsilon_{jdb}(\mathbf{z}) = e^{-ik\mu(\mathbf{z})} R_j^d(\mathbf{z}) N_j(\mathbf{z}_\Gamma) \left(0.5^{b-1} (1 + \xi_0 \xi)^{b-1} \right) & \text{for } d > 1 \end{cases} \quad (2.155)$$

The definition of the approximation in the infinite elements can be further simplified by noting that the summation over the indices could be combined to give a summation over a single index α^I say which varied from 1 to n_d^I where n_d^I is the total number of degree of freedom of the model in the outer region (the sum of the number of unknowns at each infinite node). The way in which the index is assigned to the single index α^I is unimportant provided that there is a one to one mapping. The approximation in the infinite outer region then becomes

$$\tilde{\phi}_h^I(\mathbf{z}, \omega, M_0) = \sum_{\alpha^I=1}^{n_d^I} \Phi_{\alpha^I}^I e_{\alpha^I} \quad (2.156)$$

where $\Phi_{\alpha^I}^I$ and e_{α^I} denote Υ_{jdb} and e_{jdb} .

The infinite weighting functions ($W_{\alpha^I}^I$) are chosen to be the complex conjugates of the infinite shape functions ($\Phi_{\alpha^I}^I$) following a conjugated Galerkin scheme. This choice leads to the cancellation of wavelike terms ($e^{\pm ik\mu}$) in the infinite integrals.

$$W_{\alpha^I}^I(\mathbf{z}, \omega, M_0) = G(\mathbf{z}) \left(\Phi_{\alpha^I}^I(\mathbf{z}, \omega, M_0) \right)^* \quad (2.157)$$

where G is the geometric factor chosen to conduct to proper integrals for the infinite elements.

$$G(\mathbf{z}, \mathbf{M}_0) = \left(\frac{H_{1,i}}{\sqrt{(z - z_0)^2 + \beta^2 (r - r_0)^2}} \right)^q \quad q \geq 3 \quad (2.158)$$

2.10 Summary

In this chapter, we expose the Mapped Finite and Infinite Partition of Unity Method applied to convected wave propagation applications. The model problem is first presented in its strong form from which the variational formulation is derived.

A review of numerical methods in the field of acoustic propagation is presented for cavity or unbounded domain applications. The Partition of Unity Method is applied to the variational formulation of the convected wave equation. We restricte the enrichment to be polynomial, all the reasons for this choice are explained. The concept of Infinite Elements, originally designed for the Finite Element Method, is updated to be consistent to the Partition of Unity Finite Element Method.

The developments are presented to analyse three-dimensional and axisymmetric applications.

References

1. Ph. Bouillard, F. Ihlenburg, Error estimation and adaptivity for the finite element solution in acoustics: 2D and 3D applications, *Comput. Methods Appl. Mech. Engrg.* 176 (1999) 147-163.
2. F. Ihlenburg, I. Babuška, Dispersion analysis and error estimation of Galerkin finite element methods for the Helmholtz equation, *Int. J. Numer. Methods Eng.* 38 (1995) 3745-3774.
3. J.T. Oden, S. Prudhomme, L. Demkowicz, A posteriori error estimation for acoustic wave propagation problems, *Arch. Comput. Meth. Engng.* 12 (2005) 343-389.
4. F. Ihlenburg, I. Babuška, Finite element solution of the Helmholtz equation with high wave number part II : the h-p version of the FEM, *SIAM J. Numer. Anal.* 34 (1997) 315-358.
5. O.C. Zienkiewicz, Achievements and some unsolved problems of the finite element method, *Int. J. Numer. Methods Eng.* 47 (2000) 9-28.
6. L.L. Thompson, A review of finite element methods for time-harmonic acoustics, *J. Acoust. Soc. Am.* 119 (2006) 1315-1330.
7. J.M. Melenk, I. Babuška, The partition of unity finite element method: basic theory and applications, *Comput. Methods Appl. Mech. Engrg.* 139 (1996) 289-314.
8. I. Babuška, J.M. Melenk, The Partition of Unity Method, *Int. J. Numer. Methods Eng.* 40 (1997) 727-758.
9. O. Laghrouche, P. Bettess, R. J. Astley, Modeling of short wave diffraction problems using approximating systems of plane waves, *Int. J. Numer. Methods Eng.* 54 (2002) 1501-1533.
10. Th. Strouboulis, I. Babuška, R. Hidayat, The generalized finite element method for Helmholtz equation: Theory, computation, and open problems, *Comput. Methods Appl. Mech. Engrg.* 195 (2006) 4711-4731.
11. Th. Strouboulis, R. Hidayat, I. Babuška, The generalized finite element method for Helmholtz equation Part II: Effect of choice of handbook functions, error due to absorbing boundary conditions and its assessment, *Comput. Methods Appl. Mech. Engrg.* 197 (2008) 364-380.
12. Th. Strouboulis, K. Copps, I. Babuška, The generalized finite element method, *Comput. Methods Appl. Mech. Engrg.* 190 (2001) 4081-4193.
13. Th. Strouboulis, I. Babuška, K. Copps, The design and analysis of the generalized finite element method, *Comput. Methods Appl. Mech. Engrg.* 181 (2000) 43-69.
14. C. Farhat, I. Harari, L.P. Franca, The discontinuous enrichment method, *Comput. Methods Appl. Mech. Engrg.* 190 (2001) 6455-6479.
15. B. Pluymers, W. Desmet, D. Vandepitte, P. Sas, Application of an efficient wave-based prediction technique for the analysis of vibro-acoustic radiation problems, *J. Comput. Appl. Math.* 168 (2004) 353-364.
16. P. Gamallo, R.J. Astley, A comparison of two Trefftz-type methods: The ultraweak variational formulation and the least-squares method, for solving shortwave 2-D Helmholtz problems, *Int. J. Numer. Methods Eng.* 71 (2007) 406-432.
17. P. Gamallo, R.J. Astley, The partition of unity finite element method for short wave acoustic propagation on non-uniform potential flows, *Int. J. Numer. Methods Eng.* 65 (2006) 425-444.
18. T. Huttunen, P. Gamallo, R.J. Astley, Comparison of two wave element methods for the Helmholtz problem, *Commun. Numer. Meth. Engng.* Article in Press (2008) doi:10.1002/cnm1102.
19. T. Huttunen, P. Monk, J.P. Kaipio, Computational aspects of the ultra weak variational formulation, *J. Comput. Phys.* 182 (2002) 27-46.
20. T. Huttunen, J.P. Kaipio, P. Monk, An ultra weak method for acoustic fluid-solid interaction, *J. Comput. Appl. Math.* 213 (2008) 166-185.

21. P. Monk, D.-Q. Wang, A least squares method for the Helmholtz equation, *Comput. Methods Appl. Mech. Engrg.* 175 (1999) 121-136.
22. R. Sevilla, S. Fernández-Méndez, A. Huerta, NURBS-enhanced finite element method (NEFEM), *Int. J. Numer. Methods Eng. Early View* (2008) doi: 10.1002/nme.2311
23. E. Chadwick, P. Bettess, O. Laghrouche, Diffraction of short waves modeled using new mapped wave envelope finite and infinite elements, *Int. J. Numer. Methods Eng.* 45 (1999) 335-354.
24. E. De Bel, P. Villon, Ph. Bouillard, Forced vibrations in the medium frequency range solved by a partition of unity method with local information, *Int. J. Numer. Methods Eng.* 162 (2004) 1105-1126.
25. L. Hazard, Ph. Bouillard, Structural dynamics of viscoelastic sandwich plates by the partition of unity finite element method, *Comput. Methods Appl. Mech. Engrg.* 196 (2007) 4101-4116.
26. T.J.R. Hughes, J.A. Cotrell, Y. Bazilevs, Isogeometric analysis: CAD, finite elements, NURBS, exact geometry and mesh refinement, *Comput. Methods Appl. Mech. Engrg.* 194 (2005) 4135-4195.
27. B. Szabó, A. Düster, E. Rank, The p-version of the finite element method, in: E. Stein, R. de Borst, T.J.R. Hughes (Eds.), *Fundamentals, Encyclopedia of Computational Mechanics*, vol. 1, Wiley, New York, 2004 (Chapter 5).
28. R.J. Astley, P. Gamallo, Special short wave elements for flow acoustics, *Comput. Methods Appl. Mech. Engrg.* 194 (2005) 341-353.
29. R.J. Astley, P. Gamallo, The Partition of Unity Finite Element Method for Short Wave Acoustic Propagation on Non-uniform Potential Flows, *Int. J. Numer. Methods Eng.* 65 (2006) 425-444.
30. R.J. Astley, G.J. Macaulay, J.-P. Coyette, L. Cremers, Three-dimensional wave-envelope elements of variable order for acoustic radiation and scattering. Part I. Formulation in the frequency domain, *J. Acoust. Soc. Am.* 103 (1998) 49-63.
31. R.J. Astley, J.-P. Coyette, Conditioning of infinite element schemes for wave problems, *Commun. Numer. Meth. Engrg.* 17 (2001) 31-41.
32. D. Dreyer, O. von Estorff, Improved conditioning of infinite elements for exterior acoustics, *Int. J. Numer. Methods Eng.* 58 (2003) 933-953.
33. J.J. Shirron, I. Babuška, A comparison of approximate boundary conditions and infinite element methods for exterior Helmholtz problems, *Comput. Methods Appl. Mech. Engrg.* 164 (1998) 121-139
34. D. Dreyer, Efficient infinite elements for exterior acoustics, PhD thesis, Shaker Verlag, Aachen, 2004.
35. W. Eversman, Mapped infinite wave envelope elements for acoustic radiation in a uniformly moving medium, *J. Sound Vib.* 224 (1999) 665-687.
36. S.J. Rienstra, W. Eversman, A numerical comparison between the multiple-scales and finite-element solution for sound propagation in lined flow ducts, *J. Fluid Mech.* 437 (2001) 367-384.
37. S.J. Rienstra, Sound transmission in slowly varying circular and annular lined ducts with flow, *J. Fluid Mech.* 380 (1999) 279-296.
38. S.J. Rienstra, The Webster equation revisited, 8th AIAA/CEAS Aeroacoustic conference (2002) AIAA 2002-2520.
39. M.K. Myers, On the acoustic boundary condition in the presence of flow, *J. Sound Vib.* 71 (1980) 429-434.
40. T. Mertens, Meshless modeling of acoustic radiation in infinite domains, *Travail de spécialisation, Université Libre de Bruxelles (U.L.B.)*, 2005.
41. W. Eversman, The boundary condition at an impedance wall in a non-uniform duct with potential mean flow, *J. Sound Vib.* 246 (2001) 63-69.
42. B. Regan, J. Eaton, Modeling the influence of acoustic liner non-uniformities on duct modes, *J. Sound Vib.* 219 (1999) 859-879.
43. H.-S. Oh, J.G. Kim, W.-T. Hong, The Piecewise Polynomial Partition of Unity Functions for the Generalized Finite Element Methods, *Comput. Methods Appl. Mech. Engrg.* Accepted manuscript (2008), doi: 10.1016/j.cma.2008.02.035.
44. Free Field Technologies, Actran user's manual, <http://fft.be>.
45. University of Florida, Department of Computer and Information Science and Engineering, <http://www.cise.ufl.edu/research/sparse/umfpack/>
46. T.A. Davis, A column pre-ordering strategy for the unsymmetric-pattern multifrontal method, *ACM Transactions on Mathematical Software* 30 (2004) 165-195.
47. T.A. Davis, Algorithm 832: UMFPACK, an unsymmetric-pattern multifrontal method, *ACM Transactions on Mathematical Software* 30 (2004) 196-199.
48. T.A. Davis and I.S. Duff, A combined unifrontal/multifrontal method for unsymmetric sparse matrices, *ACM Transactions on Mathematical Software* 25 (1999) 1-19.

49. T.A. Davis and I.S. Duff, An unsymmetric-pattern multifrontal method for sparse LU factorization, *SIAM Journal on Matrix Analysis and Applications* 18 (1997) 140-158.
50. A. Hirschberg, S.W. Rienstra, An introduction to aeroacoustics, Eindhoven University of Technology (2004).
51. G. Warzée, *Mécanique des solides et des fluides*, Université Libre de Bruxelles (2005).
52. M.J. Crocker, *Handbook of acoustics*, Wiley-Interscience, New York (1998).
53. R. Sugimoto, P. Bettess, J. Trevelyan, A numerical integration scheme for special quadrilateral finite elements for the helmholtz equation, *Commun. Numer. Meth. Engng.* 19 (2003) 233-245.
54. G. Gabard, R.J. Astley, A computational mode-matching approach for sound propagation in three-dimensional ducts with flow, *J. Sound Vib.* Article in Press (2008) doi:10.1016/j.jsv.2008.02.015.
55. C. Farhat, I. Harari, U. Hetmaniuk, A discontinuous Galerkin method with Lagrange multipliers for the solution of Helmholtz problems in the mid-frequency regime, *Comput. Methods Appl. Mech. Engrg.* 192 (2003) 1389-1419.
56. C.L. Morfey, Acoustic energy in non-uniform flows, *J. Sound Vib.* 14 (1971) 159-170.
57. F. Magoules, I. Harari (editors), Special issue on Absorbing Boundary Conditions, *Comput. Methods Appl. Mech. Engrg.* 195 (2006) 3354-3902.
58. M. Fischer, U. Gauger, L. Gaul, A multipole Galerkin boundary element method for acoustics, *Engineering Analysis with Boundary Elements* 28 (2004) 155-162.
59. J.-P. Bérenger, Three-dimensional Perfectly Matched Layer for the absorption of electromagnetic waves, *J. Comput. Phys.* 127 (1996) 363-379.
60. C. Michler, L. Demkowicz, J. Kurtz, D. Pardo, Improving the performance of Perfectly Matched Layers by means of hp-adaptivity, *Numerical Methods for Partial Differential Equations* 23 (2007) 832-858.
61. A. Bayliss, E. Turkel, Radiation boundary conditions for wave-like equations, *Comm. Pure Appl. Math.* 33 (1980) 707-725.
62. B. Engquist, A. Majda, Radiation boundary conditions for acoustic and elastic wave calculations, *Comm. Pure Appl. Math.* 32 (1979) 313-357.
63. K. Feng, Finite element method and natural boundary reduction, *Proceedings of the International Congress of Mathematicians*, Warsaw (1983) 1439-1453.
64. D. Givoli, B. Neta, High-order non-reflecting boundary scheme for time-dependent waves, *J. Comput. Phys.* 186 (2003) 24-46.
65. T. Hagstrom, A. Mar-Or, D. Givoli, High-order local absorbing conditions for the wave equation: Extensions and improvements, *J. Comput. Phys.* 227 (2008) 3322-3357.
66. T. Hagstrom, T. Warburton, A new auxiliary variable formulation of high-order local radiation boundary conditions: corner compatibility conditions and extensions to first order systems, *Wave Motion* 39 (2004) 327-338.
67. A. Hirschberg, S.W. Rienstra, An introduction to aeroacoustics, Eindhoven university of technology (2004).
68. V. Lacroix, Ph. Bouillard, P. Villon, An iterative defect-correction type meshless method for acoustics, *Int. J. Numer. Meth. Engng* 57 (2003) 2131-2146.
69. T. Mertens, P. Gamallo, R. J. Astley, Ph. Bouillard, A mapped finite and infinite partition of unity method for convected acoustic radiation in axisymmetric domains, *Comput. Methods Appl. Mech. Engrg.* 197 (2008) 4273-4283.
70. G. Gabard, Discontinuous Galerkin methods with plane waves for time harmonic problems, *J. Comput. Phys.* 225 (2007) 1961-1984.
71. L. Hazard, Design of viscoelastic damping for vibration and noise control: modeling, experiments and optimisation, PhD thesis, Université Libre de Bruxelles (2007).
72. G. Gabard, R.J. Astley, M. Ben Tahar, Stability and accuracy of finite element methods for flow acoustics. I: general theory and application to one-dimensional propagation, *Int. J. Numer. Meth. Eng.* 63, (2005) 947-973.
73. G. Gabard, R.J. Astley, M. Ben Tahar, Stability and accuracy of finite element methods for flow acoustics. II: Two-dimensional effects, *Int. J. Numer. Meth. Eng.* 63 (2005) 974-987.
74. A. Goldstein, Steady state unfocused circular aperture beam patterns in non attenuating and attenuating fluids, *J. Acoust. Soc. Am.* 115 (2004) 99-110.
75. T. Douglas Mast, F. Yu, Simplified expansions for radiation from baffled circular piston, *J. Acoust. Soc. Am.* 118 (2005) 3457-3464.
76. T. Hasegawa, N. Inoue, K Matsuzawa, A new rigorous expansion for the velocity potential of a circular piston source, *J. Acoust. Soc. Am.* 74 (1983) 1044-1047.
77. R.J. Astley, A finite element, wave envelope formulation for acoustical radiation in moving flows, *J. Sound Vib.* 103 (1985) 471-485.
78. J.M. Tyler, T.G. Sofrin, Axial flow compressor noise studies, *SAE Transactions* 70 (1962) 309-332.

79. M.C. Duta, M.B. Giles, A three-dimensional hybrid finite element/spectral analysis of noise radiation from turbofan inlets, *J. Sound Vib.* 296 (2006) 623-642.
80. H.H. Brouwer, S.W. Rienstra, Aeroacoustics research in Europe: The CEAS-ASC report on 2007 highlights, *J. Sound Vib.* Article in Press (2008) doi:10.1016/j.jsv.2008.07.020.
81. http://en.wikipedia.org/wiki/Aircraft_noise, 4th September 2008.
82. Y. Park, S. Kim, S. Lee, C. Cheong, Numerical investigation on radiation characteristics of discrete-frequency noise from scarf and scoop aero-intakes, *Appl. Acoust.* Article in press (2008) doi:10.1016/j.apacoust.2007.09.005.
83. General Electric Company, <http://www.ge.com>, http://www.turbokart.com/about_ge90.htm, 4th September 2008.
84. R.J. Astley, J.A. Hamilton, Modeling tone propagation from turbofan inlets - The effect of extended lip liner, AIAA paper 2002-2449 (2002).
85. V. Decouvreur, Updating acoustic models: a constitutive relation error approach, PhD thesis, Université Libre de Bruxelles (2008).
86. P.A. Nelson, O. Kirkeby, T. Takeuchi, and H. Hamada, Sound fields for the production of virtual acoustic images, Letters to the editor, *J. Sound Vib.* 204 (1999) 386-396.
87. Y. Reymen, W. De Roeck, G. Rubio, M. Bealmans, W. Desmet, A 3D Discontinuous Galerkin Method for aeroacoustic propagation, Proceedings of the 12th International Congress on Sound and Vibration 2005.
88. G. Gabard, Exact integration of polynomial-exponential products with an application to wave based numerical methods, *Commun. Numer. Meth. Engng* (2008) doi: 10.1002/cnm.1123.
89. New York University, http://math.nyu.edu/faculty/greengar/shortcourse_fmm.pdf, 1st december 2008.